Chem Soc Rev

REVIEW ARTICLE

View Article Online
View Journal | View Issue

Cite this: *Chem. Soc. Rev.*, 2016, **45**, 203

Switchable Fe/Co Prussian blue networks and molecular analogues

David Aguilà,*[ab] Yoann Prado,[ab] Evangelia S. Koumousi,[abcd] Corine Mathonière*[cd] and Rodolphe Clérac*[ab]

Received 18th April 2015

DOI: 10.1039/c5cs00321k

www.rsc.org/chemsocrev

With the long term objective to build the next generation of devices from the molecular scale, scientists have explored extensively in the past two decades the Prussian blue derivatives and their remarkable physico-chemical properties. In particular, the exquisite Fe/Co system displays tuneable optical and magnetic behaviours associated with thermally and photo-induced metal-to-metal electron transfer processes. Recently, numerous research groups have been involved in the transfer of these electronic properties to new Fe/Co coordination networks of lower dimensionality as well as soluble molecular analogues in order to facilitate their manipulation and integration into devices. In this review, the most representative examples of tridimensional Fe/Co Prussian blue compounds are described, focusing on the techniques used to understand their photomagnetic properties. Subsequently, the different strategies employed toward the design of new low dimensional Prussian blue analogues based on a rational molecular building block approach are discussed emphasizing the advantages of these functional molecular systems.

1. Introduction

Molecule-based materials have attracted great interest in the last two decades due to exciting and novel features originating from the molecular level.[1–4] In conjunction with such development, research has focused on the control of their optical and magnetic properties by an external stimulus different from the

[a] *CNRS, CRPP, UPR 8641, F-33600 Pessac, France. E-mail: clerac@crpp-bordeaux.cnrs.fr, aguila@crpp-bordeaux.cnrs.fr; Tel: +33 5 56 84 56 50*
[b] *Univ. Bordeaux, CRPP, UPR 8641, F-33000 Pessac, France*
[c] *CNRS, ICMCB, UPR 9048, F-33600 Pessac, France. E-mail: Corine.Mathoniere@icmcb.cnrs.fr; Tel: +33 5 40 00 26 82*
[d] *Univ. Bordeaux, ICMCB, UPR 9048, F-33600 Pessac, France*

David Aguilà

David Aguilà (born in 1984, Barcelona, Spain) received his PhD at the Universitat de Barcelona in 2013 under the supervision of Dr G. Aromí. His PhD work was dedicated to the design of magnetic coordination complexes for their application in quantum computing. During this period, he complemented his research with a stay in Prof. A. Bond's Electrochemistry Group at Monash University, Melbourne (2009), and in Prof. J. Long's Group at University of California Berkeley, California (2011). Currently, he is working as a postdoctoral researcher with Dr R. Clérac in the M_3 team (CRPP), focusing on the development of new photomagnetic molecule-based materials.

Yoann Prado

Yoann Prado (born in 1980, Paris, France) received his PhD in 2010 under the supervision of Dr L. Catala and Prof. T. Mallah (ICMMO) at the Université Paris-Sud. Then he worked for two years in the group of Prof. E. Coronado (ICMol) at Universitat de Valencia, Spain. In 2013, he came back to France to work for one year with Dr Jérôme Fresnais in Phenix group and Dr Laurent Lisnard (IPCM) at Université Pierre et Marie Curie, Paris. Since 2014, he has been a postdoctoral fellow in the group of Dr R. Clérac (M_3 team, CRPP Pessac, France). His current subjects of interest are coordination chemistry, nano-heterostructures synthesis and magnetism.

magnetic field such as temperature, light, pressure or electrical field.[5,6] The possibility to control the magnetization with light is particularly appealing for potential applications in information storage, where magnetic molecules can be used as molecular bits and addressed by these stimuli. Amongst the molecules displaying such properties, Fe^{II} complexes exhibiting spin crossover phenomenon were the first to show a modification of their spin state through light irradiation at low temperature.[4,7] Another important class of molecular switches allowing such control with light is based on intramolecular electron transfer processes.[5] In these molecules, the presence of electronic donor and acceptor moieties promotes a reversible transfer of one electron between the two sites through temperature change and/or low temperature photo-excitation. As for spin crossover materials, the modification of the optical and magnetic states by light irradiation allows magneto-optical bistability. Different donor/acceptor couples have been considered in molecular compounds, such as radicals or complexes, implying an electron transfer (ET) between an organic moiety (radical/ligand) and a metal center[8] or between two metal ions.[9,10] In this later case, Fe/Co Prussian blue analogues (PBAs) have emerged as one of the most interesting systems, due to their outstanding photo-switchable physical properties. These cyanido-bridged bimetallic tridimensional coordination networks, with general formula $A_xCo_y[Fe(CN)_6]\cdot nH_2O$ (A: alkaline ion), can display both optical and magnetic bistability due to a reversible metal-to-metal electron transfer process between the cobalt and iron centres, switching between paramagnetic (Fe^{III}_{LS}–CN–Co^{II}_{HS}) and diamagnetic (Fe^{II}_{LS}–CN–Co^{III}_{LS}) configurations (Scheme 1; with LS: low Spin and HS: high Spin). Due to the different electronic distribution of the cobalt centre (HS or LS), this phenomenon has been named as charge-transfer-induced spin transition (CTIST),[11] although the mechanism related to this electronic reorganization is still under debate. This reversible process can be triggered by a change of the temperature (thermally induced electron transfer) as well as by irradiation at low temperatures (photo-induced electron transfer). On the other hand, transferring this remarkable magnetic and optical bistability into systems with lower dimensionality (2D, 1D or 0D) has emerged as an attractive research goal to develop new materials that can be easily manipulated and studied. The use of blocking ligands, which limit or impede the growth of the coordination network, allows a fine and controlled reduction of the structural dimensionality resulting in discrete Fe/Co Prussian blue molecular analogues.[12–16] In most of the reported cases, these species are obtained from the reaction of cyanido/Fe^{III} and Co^{II} building blocks of general formula $[Fe^{III}L(CN)_p]^{n-}$ and $[Co^{II}L'(S)_q]^{m+}$

Evangelia S. Koumousi

Evangelia S. Koumousi (born in 1989, Korinthos, Greece) received her Master degree from the University of Patras (Greece) in 2012 under the supervision of Prof. S. P. Perlepes and Dr Th. C. Stamatatos, focusing on the synthesis and characterization of Mn^{III}-based coordination complexes with oximate ligands. Currently she is preparing a PhD degree at the University of Bordeaux working on the design of photomagnetic Fe/Co cyanido-bridged discrete systems under the supervision of Dr R. Clérac at the Centre de Recherche Paul Pascal (CRPP, France) and Prof. C. Mathonière at the Institut de Chimie de la Matière Condensée de Bordeaux (ICMCB, France).

Corine Mathonière

Corine Mathonière (born in 1968, Montluçon, France) received her PhD at the University Paris XI under the supervision of Prof. O. Kahn and Prof. J.-J. Girerd. After a post-doctoral stay in the group of Prof. P. Day at the Royal Institution of Great Britain in London, she was hired as an associate professor in 1994 at the Université Bordeaux 1 and at the Institut de Chimie de la Matière Condensée de Bordeaux (ICMCB, Bordeaux, France). In 2010, she was promoted professor and got a junior position at the Institut Universitaire de France. She played a major role in the discovery of the photomagnetic effects in Cu–Mo compounds and has developed with co-workers a new research area focused on electron transfer compounds.

Rodolphe Clérac

Rodolphe Clérac (born in 1971, Versailles, France) received his PhD at the University of Bordeaux 1 under the supervision of Prof. C. Coulon in 1997. After a short post-doctoral stay in the group of Prof. O. Kahn (ICMCB, Bordeaux, France), he joined in 1998 Prof. K. R. Dunbar's group at Michigan State University (East Lansing, Michigan, USA) and in 1999, he moved with Dunbar's group to Texas A&M University (College Station, Texas, USA) where he collaborated with Prof. F. A. Cotton. Since 2000, he has established his research group (Molecular Materials & Magnetism, M_3) at the Centre de Recherche Paul Pascal (CNRS) interested in the synthesis and physical properties of molecular materials.

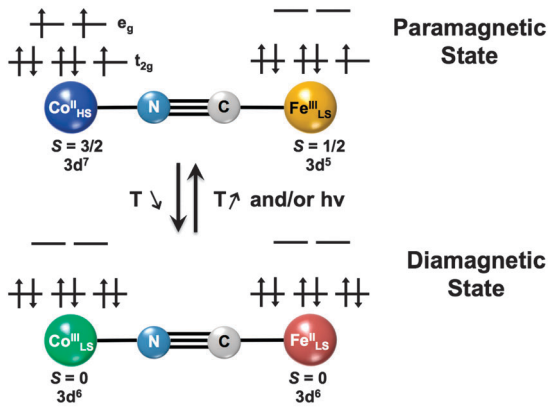

Scheme 1 Interconversion between the paramagnetic (Fe^{III}_{LS}–CN–Co^{II}_{HS}) and diamagnetic (Fe^{II}_{LS}–CN–Co^{III}_{LS}) electronic configurations due to thermally and photo-induced metal-to-metal electron transfer processes.

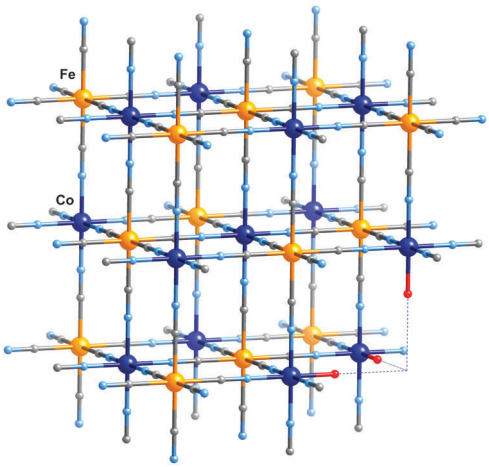

Fig. 1 Schematic representation of a Fe/Co Prussian blue network with formula $A_xCo_y[Fe(CN)_6]\cdot nH_2O$ (A: alkaline ions, which have been omitted for clarity; C: grey; N: light blue; Co: blue; Fe: yellow; O: red).

respectively (L, L′: ligands and S: solvent molecules). The presence of the ligands affords also a good solubility of the final complexes in organic solvents, consequently allowing the study of electron transfer processes in solution. More importantly and in contrast to the 3D Prussian blue materials, the design of discrete species guarantees a well-defined environment of the cobalt coordination sphere, that favours a full electron transfer in these molecular compounds. In addition, the versatility of coordination chemistry allows the fine-tuning of the building block redox potentials through ligand design and molecular engineering, and thus the control of the electron transfer properties. Hence, the reduction of the structural dimensionality in this family of Fe/Co Prussian blue analogues can obviously lead to interesting model systems essential to improve our comprehension of these metal-to-metal electron transfer processes.

In this review article, the most representative examples of tridimensional $A_xCo_y[Fe(CN)_6]\cdot nH_2O$ Prussian blue compounds are described, focusing on their photomagnetic switchable properties and how those are influenced by their chemical composition. Subsequently, the different strategies employed toward the design of new low dimensional Prussian blue systems based on a rational molecular building block approach are discussed emphasizing the advantages and potential applications of these functional molecular analogues.

2. Switchable Fe/Co Prussian blue networks

The Prussian blue materials has been widely studied due to their appealing electronic and magnetic properties. The original Prussian blue, $Fe^{III}_4[Fe^{II}(CN)_6]_3\cdot 14H_2O$, is a Robin and Day's class II mixed-valence system.[17,18] The intense and characteristic blue colour of this pigment originates from a metal-to-metal electron transfer band around 700 nm due to the weak electron delocalization between the metallic centres through the cyanide bridge.[17] This electronic delocalization is also responsible for the superexchange interactions between high spin Fe^{III} ions, although separated by 10.17 Å through the diamagnetic $[Fe^{II}(CN)_6]^{4-}$ unit,[19–21] leading to a ferromagnetic order below 5.2 K. Intense research efforts in the 1990s have led to the rationalization of the magnetic properties of Prussian blue analogues (PBAs), allowing the synthesis of room temperature molecule-based magnets.[3]

The Fe/Co Prussian blue materials have a general formula $A_xCo_y[Fe(CN)_6]\cdot nH_2O$ (A: Na^+, K^+, Cs^+, Rb^+) and form a neutral tridimensional network (Fig. 1) obtained from the reaction of hexacyanidoferrate(III) ($[Fe^{III}(CN)_6]^{3-}$) with cobalt(II) centres in water ($[Co^{II}(OH_2)_6]^{2+}$), in presence of alkaline ions A^+. These coordination networks adopt a face-centred cubic (fcc) structure in the *Fm*3*m* space group, with a cell parameter close to 10 Å depending on the oxidation state of the metallic ions and the nature of alkaline ions.[22–24] The vertices and the centres of the faces of the cubic unit cell are occupied by the Fe^{III} ions, while Co^{II} ions are located at the octahedral sites (Fig. 1). Both metal centres are linked by cyanide bridges with Fe^{III} and Co^{II} being coordinated by carbon and nitrogen, respectively. The corresponding ligand field of both donor atoms leads to low spin Fe^{III}_{LS} and high spin Co^{II}_{HS} configurations. Zeolitic water molecules form a hydrogen-bonded network in the interstitial sites, where alkaline ions are also inserted. Depending on the amount of alkaline ions introduced, the stoichiometry of the compound can vary. The electro-neutrality of the network is ensured by adjusting the number of $[Fe^{III}(CN)_6]^{3-}$ vacancies (□), and the coordination sphere of the neighbouring Co^{II} sites is completed by water molecules (as shown on the right bottom corner of structure in Fig. 1; note that each missing $[Fe^{III}(CN)_6]^{3-}$ unit is leading to the coordination of six additional water molecules). Hence, in the crystal, such vacancies (inhomogeneously distributed through the network) are responsible for a variety of coordination environments around the Co^{II} ions leading to an average $CoN_{6-p}O_p$ coordination sphere. These different environments around the Co^{II} site are of particular importance

for the electron transfer properties, which are correlated to the redox potential of the two metal centres.[25] The replacement of a nitrogen atom from the cyanide ligand by a water molecule increases the redox potential of the cobalt centre. Therefore depending on the amount of water on the Co site, the Co redox potential can be significantly lower or higher than the Fe one, stabilizing Fe^{II}/Co^{III} or Fe^{III}/Co^{II} states respectively. This is only when the redox potential of the Co site is slightly lower than the Fe one, that the Fe^{III}/Co^{II} paramagnetic excited state becomes thermally and optically accessible above the Fe^{II}/Co^{III} ground state.[25] Hence, the electron transfer phenomena in this Fe/Co Prussian blue analogue can be easily tuned through modification of the vacancies, directly in link with the quantity of alkaline ions inserted in the network.

2.1. First evidence of photo-induced magnetization

About twenty years ago, the control of the spontaneous magnetization of molecule-based materials by an optical stimulus was one of the main challenges within the molecular magnetism community. As previously discussed, the unique magnetic properties observed in some of the Prussian blue analogues make them potential candidates to develop such new systems with a light control of the magnetic properties. The breakthrough was achieved by Hashimoto, Fujishima and co-workers who synthesized a new Fe/Co Prussian blue analogue with the formula $K_{0.2}Co_{1.4}[Fe(CN)_6]\cdot 6.9H_2O$ (**1**).[22,26] As for other related PBAs,[19] a face-centred *Fm3m* cubic structure was observed by powder X-ray diffraction, with a unit cell parameter a = 10.28 Å. The infrared spectrum carried out at 12 K showed two bands at 2162 and 2116 cm^{-1} that were ascribed to the cyanide stretching in Fe^{III}–CN–Co^{II} and Fe^{II}–CN–Co^{III} configurations, respectively (see Table 1). The higher intensity of the former band suggested the main oxidation of both metal ions, while the presence of the diamagnetic Fe^{II}–CN–Co^{III} units was attributed to a spontaneous metal-to-metal electron transfer due to the introduction of K^+ ions in the structure. Magnetization measurements revealed a tridimensional ferrimagnetic order in the compound with a Curie temperature of about 16 K. In order to investigate the photo-induced magnetic effect, the material was irradiated at 5 K with red light (660 nm), observing for the first time an enhancement of the magnetization, and an increase of the ordering temperature to 19 K. Interestingly, when the temperature was increased back to 150 K, the sample relaxed to its original state with a para/ferrimagnetic transition around 16 K. These unprecedented results demonstrated that the magnetization can be changed under light irradiation, and that the initial properties can be restored by thermal treatment. Accordingly, the infrared spectrum after irradiation at 12 K showed concomitantly a decrease of the peak at 2116 cm^{-1} and an increase of the peak at 2162 cm^{-1}. Taking into the account the band ascription given before, these effects demonstrated that a photo-induced electron-transfer transformation from $Fe^{II}_{LS(S=0)}$–CN–$Co^{III}_{LS(S=0)}$ into $Fe^{III}_{LS(S=1/2)}$–CN–$Co^{II}_{HS(S=3/2)}$ was possible and induced an increase of the paramagnetic site number in the material, with a consequent enhancement of the magnetization value. Therefore, it was established that the presence of the diamagnetic Fe^{II}–CN–Co^{III} units were responsible of the photo-induced effect observed in **1**. Moreover, the authors also proved that the photo-enhancement of the magnetization was partially reversible irradiating the compound with a blue light (450 nm). Sequence of irradiation alternating red and blue lights was also reported to illustrate the remarkable bistability of this system at 5 K. The Science paper of Hashimoto, Fujishima and co-workers in 1996[22] that summarizes these results, is thus considered to be the first report of a tuneable magnetism based on a photo-induced metal-to-metal electron-transfer process.

2.2. Tuning the photomagnetic behaviour of the tridimensional Fe/Co PBAs

After the discovery of the photo-induced magnetization in $K_{0.2}Co_{1.4}[Fe(CN)_6]\cdot 6.9H_2O$, several other Fe/Co Prussian blue

Table 1 Characteristics of the Fe/Co Prussian blue analogues and their electron-transfer (ET) properties

Compound (number in text)	% Vacancies [□]	$CoN_{6-p}O_p$	$\bar{\nu}_{CN}$[a] (cm^{-1})	ET with temperature	ET with light	EXAFS	XANES	Ref.
$Co_{1.5}[Fe(CN)_6]\cdot 6H_2O$ (**3**)	33	CoN_4O_2	2163	Non active	Non active	Yes	Yes	31 and 43
$K_{0.04}Co_{1.48}[Fe(CN)_6]\cdot 6.8H_2O$ (**4**)	33	$CoN_{4.1}O_{1.9}$	2156, 2090	Non active	Non active	—	—	23
$K_{0.2}Co_{1.4}[Fe(CN)_6]\cdot 6.9H_2O$ (**1**)	29	$CoN_{4.3}O_{1.7}$	2162, 2116	Non active	Active	—	—	22
$K_{0.4}Co_{1.3}[Fe(CN)_6]\cdot 4.2H_2O$ (**10**)	23	$CoN_{4.6}O_{1.4}$	—	Active (280 K)	—	Yes	Yes	43
$K_{0.4}Co_{1.3}[Fe(CN)_6]\cdot 5H_2O$ (**8**)	23	$CoN_{4.6}O_{1.4}$	2135	Non active	Active	Yes	Yes	29 and 43
$Na_{0.07}Co_{1.5}[Fe(CN)_6]\cdot 6.3H_2O$	33	CoN_4O_2	2155, 2089	Non active	Non active	—	—	11
$Na_{0.37}Co_{1.37}[Fe(CN)_6]\cdot 4.8H_2O$	27	$CoN_{4.4}O_{1.6}$	2155, 2089	Active (180/220 K)	Active	—	—	11
$Na_{0.4}Co_{1.3}[Fe(CN)_6]\cdot 5H_2O$ (**9**)	23	$CoN_{4.6}O_{1.4}$	2160	Active (260 K)	—	Yes	Yes	29 and 43
$Na_{0.43}Co_{1.35}[Fe(CN)_6]\cdot 4.6H_2O$ (**7**)	26	$CoN_{4.4}O_{1.6}$	—	Active (213/232 K)	Active	—	—	40 and 41
$Na_{0.53}Co_{1.32}[Fe(CN)_6]\cdot 4.4H_2O$	24	$CoN_{4.5}O_{1.5}$	2155, 2089	Active (230/270 K)	Active	—	—	11
$Na_{0.60}Co_{1.26}[Fe(CN)_6]\cdot 3.9H_2O$	21	$CoN_{4.8}O_{1.2}$	2155, 2122	Active (260/300 K)	Active	—	—	11
$Na_{0.94}Co_{1.15}[Fe(CN)_6]\cdot 3H_2O$	13	$CoN_{5.2}O_{0.8}$	2122	Non active	Non active	—	—	11
$Na_{1.4}Co_{1.3}[Fe(CN)_6]\cdot 5H_2O$ (**11**)	23	$CoN_{4.6}O_{1.4}$	2100	Non active	—	Yes	Yes	29 and 43
$Rb_{0.55}Co_{1.2}[Fe(CN)_6]\cdot 3.9H_2O$ (**5**)	17	CoN_5O_1	2125	Non active	Active	—	—	23
$Rb_{0.66}Co_{1.25}[Fe(CN)_6]\cdot 4.3H_2O$ (**2**)	20	$CoN_{4.8}O_{1.2}$	2133	Non active	Active	Yes	Yes	31 and 43
$Cs_{0.1}Co_{1.43}[Fe(CN)_6]\cdot 6.4H_2O$	30	$CoN_{4.2}O_{1.8}$	2160, 2090	Non active	Weak	—	Yes	24
$Cs_{0.24}Co_{1.38}[Fe(CN)_6]\cdot 5.5H_2O$	28	$CoN_{4.3}O_{1.7}$	2160, 2090	Active (170–280 K)	Active	Yes	Yes	24 and 44
$Cs_{0.38}Co_{1.25}[Fe(CN)_6]\cdot 5H_2O$	20	$CoN_{4.8}O_{1.2}$	2105	Active (170–280 K)	Active	—	Yes	24
$Cs_{0.68}Co_{1.18}[Fe(CN)_6]\cdot 4.1H_2O$	15	$CoN_{5.1}O_{0.9}$	2100	Non active	Non active	—	Yes	24
$CsCo_{1.03}[Fe(CN)_6]\cdot 3.3H_2O$ (**6**)	3	$CoN_{5.8}O_{0.2}$	2120	Non active	Weak	—	—	23

[a] The highest intensity bands observed at room temperature are reported.

analogues were synthesized and studied to further understand the phenomena.[27–31] Parallel to the developments carried out by Hashimoto and co-workers, different studies were reported by other groups, especially by Bleuzen, Verdaguer and co-workers, in order to assess the influence of different synthetic parameters in the photo-induced magnetization.[23,24,26,32–39] In this section, some of the most representative results on this topic will be discussed.

One of the most relevant compounds studied by Hashimoto and co-workers was obtained by replacing potassium by rubidium: $Rb_{0.66}Co_{1.25}[Fe(CN)_6]\cdot 4.3H_2O$ (**2**).[31] To understand its photo-induced long-range magnetic order, the authors first characterized the compound by infrared and Mössbauer spectroscopy, and the results were compared with alkaline free analogue, $Co_{1.5}[Fe(CN)_6]\cdot 6H_2O$ (**3**). Compound **2** was found to be composed mainly of Fe^{II}–CN–Co^{III} pairs, while clear evidence for a Fe^{III}–CN–Co^{II} configuration was found for **3**. Indeed, elemental analysis suggested the following stoichiometries, $Rb_{0.66}Co_{0.25}Co[Fe(CN)_6][\square]_{0.25}\cdot 4.3H_2O$ for **2** and $Co_{0.5}Co[Fe(CN)_6][\square]_{0.5}\cdot 6H_2O$ for **3**, which implies $CoN_{4.8}O_{1.2}$ and CoN_4O_2 average cobalt coordination spheres for **2** and **3**, respectively (note that the oxygen atoms originate from the six water molecules, which are present for each vacancy). Since the ligand field for the N atom from the cyanide ligand is higher than the O atom from the water molecule, the electronic structure of both compounds turns out to be substantially different.[26] Thus, for a CoN_4O_2 environment (**3**), the ligand field of the cobalt is weak enough to stabilize the Fe^{III}_{LS}–CN–Co^{II}_{HS} configuration. In contrast, for **2**, where the average amount of nitrogen around the cobalt is higher ($CoN_{4.8}O_{1.2}$) due to fewer vacancies, the ligand field is stronger, thus stabilizing the diamagnetic Fe^{II}_{LS}–CN–Co^{III}_{LS} state. It is worth mentioning that these conclusions drawn from the ligand field theory are also perfectly in line with the discussion of the redox potentials reported by Bleuzen and co-workers in 2010 (*vide supra*).[25] The magnetic properties of both compounds further confirmed this scenario. For **3**, the ferrimagnetic order was observed below a Curie temperature of 16 K. In contrast, the χT values for **2** were much smaller, as the material is mostly composed by diamagnetic Fe^{II}_{LS}–CN–Co^{III}_{LS} pairs, and only a small amount of Co^{II} and Fe^{III} centres are responsible for the observed paramagnetism in the whole temperature range. Nevertheless when a sample of **2** was irradiated at 5 K, a remarkable increase of the magnetization was observed (Fig. 2).[31] This enhancement associated with a long-range magnetic order at 22 K confirmed the first studies on **1**[22] and the effect of the light illumination. When the sample was further heated to 150 K, the original value of the magnetization (before irradiation) was recovered. The same conclusions were obtained by infrared and Mössbauer spectroscopies after photo-excitation at 5 K and 25 K, respectively. Interestingly, no change in the infrared spectra after irradiation was observed in the thermal treatment until 70 K, demonstrating that the metastable photo-induced Fe^{III}_{LS}–CN–Co^{II}_{HS} configuration was kinetically trapped below this temperature. The recovery of the Fe^{II}_{LS}–CN–Co^{III}_{LS} configuration was observed only around 80 K, and the original spectrum was completely restored at *ca.* 120 K.

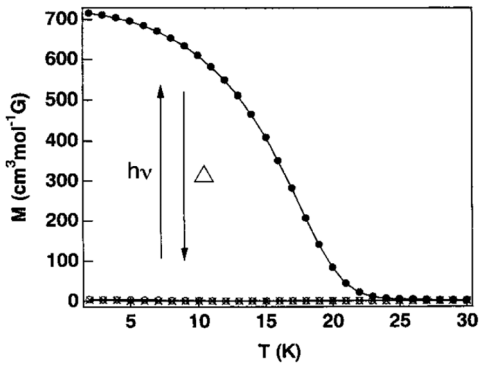

Fig. 2 Dependence of field-cooled magnetization of compound **2** with temperature under an applied field H = 0.5 mT before (empty dots) and after (black dots) light irradiation, and after the thermal treatment at 150 K (crosses). Reprinted with permission from ref. 31. Copyright 1999 American Chemical Society.

Taking into account these results, the authors proposed a possible mechanism for the light induced electron-transfer based on the CTIST process, which can explain the long-life time of the metastable state.[31] Since the change from the Fe^{II}_{LS}–CN–Co^{III}_{LS} to Fe^{III}_{LS}–CN–Co^{II}_{HS} implies a spin-forbidden transition, a possible alternative pathway was contemplated considering an intermediate Fe^{III}_{LS}–CN–Co^{II}_{LS} state. The transition between Fe^{II}_{LS}–CN–Co^{III}_{LS} and Fe^{III}_{LS}–CN–Co^{II}_{LS} is spin-allowed and could enable the following decay to Fe^{III}_{LS}–CN–Co^{II}_{HS} due to the large stability of Co^{II}_{HS}. Recovering the original Fe^{II}_{LS}–CN–Co^{III}_{LS} state turns out to be slow due to the large change in the bond distances and the spin-forbidden character of such transition. This mechanism suggests a high energy barrier, which would afford a long-lived metastable state. From these results, Hashimoto and co-workers demonstrated the importance of the presence of diamagnetic Fe^{II}_{LS}–CN–Co^{III}_{LS} pairs in the compound to allow the photo-induced magnetization.[31] At the same time, they observed that this diamagnetic motif was favoured when the number of nitrogen atoms was sufficient to guarantee a sufficiently strong ligand field around the cobalt ion.

Subsequently to Hashimoto's work, an extensive study was performed by Bleuzen, Verdaguer and co-workers through the study of three different compounds featuring different cobalt environment: $K_{0.04}Co_{1.48}[Fe(CN)_6]\cdot 6.8H_2O$ (**4**), $Rb_{0.55}Co_{1.2}[Fe(CN)_6]\cdot 13H_2O$ (**5**), and $CsCo_{1.03}[Fe(CN)_6]\cdot 3.3H_2O$ (**6**), displaying average coordination spheres close to CoN_4O_2, CoN_5O and CoN_6 respectively.[23] These environments correspond to different amount of vacancies in the material from 33% for **4**, 17% for **5**, to almost none for **6** (see Table 1). Comparing the behaviour of these three compounds, the authors demonstrated that the enhancement of the ligand field produced by five nitrogen and one oxygen atom in **5** was enough to induce a spontaneous electron transfer during the synthesis and thus to produce diamagnetic pairs in the material. Due to the existence of these diamagnetic pairs, a considerable increase of the magnetization was observed after irradiation as a signature of a photo-induced ferrimagnetic phase. However, when compound **6** (with six nitrogen atoms around the cobalt and thus a maximum of diamagnetic pairs) was measured, the effect of the light was found to be very weak. Thus, the authors confirmed that

the presence of diamagnetic pairs in the Prussian blue analogues was necessary to observe a photo-induced magnetization, but an excess of such diamagnetic pairs precludes the phenomena.[23] The hypothesis given by the authors to explain this result relies on the flexibility of the inorganic network that seems to be required to allow the necessary increase of the bond lengths during the photo-generation of the Fe^{III}_{LS}–CN–Co^{II}_{HS} pairs. When the number of diamagnetic units is too high (**6**), almost no $[Fe(CN)_6]^{3-}$ vacancies are present in the network, and thus the number of water molecules coordinated to the Co metal ions is very low. In these conditions, the network is probably relatively rigid and the photo-generation of the Fe^{III}_{LS}–CN–Co^{II}_{HS} phase is difficult to take place. This study was further complemented one year later by the same authors, who demonstrated that it was possible to induce and eventually tune the photo-induced magnetization of **6** by carefully controlling the amount of Cs^+ inserted in the structure.[24] Compounds with general formula $Cs_xCo_y[Fe(CN)_6][\square]_z{\cdot}nH_2O$ were synthesized with different x values from 0.1 to 0.68 (see Table 1). Elemental analysis showed an increase of the nitrogen amount, corresponding to a mean environment of the cobalt centre from $CoN_{4.2}O_{1.8}$ (x = 0.1, y = 1.43, z = 0.43) to $CoN_{5.1}O_{0.9}$ (x = 0.68, y = 1.18, z = 0.18), due to the decrease of z (the number of vacancies [□]). Infrared spectroscopy, powder X-ray diffraction and X-ray absorption spectroscopy (see below, Section 2.3) demonstrated the enhancement of the amount of diamagnetic Fe^{II}_{LS}–CN–Co^{III}_{LS} units with the increase of Cs^+ amount. This evidence was corroborated by measuring the magnetic susceptibility of the samples at room temperature, which was progressively reduced by the increase of Cs^+ quantity. When the Cs^+ content ranged in between x = 0.24 and 0.38, the required ligand field at the cobalt ion was empirically achieved resulting in the presence of a thermally induced electron transfer when decreasing the temperature. In contrast, when the samples were irradiated with light, the highest efficiency for the photo-induced process was observed for x between 0.38 and 0.68. Thus, this range turned out to be the best compromise between the amount of Fe^{II}_{LS}–CN–Co^{III}_{LS} diamagnetic pairs and the number of vacancies [□], providing the adequate network flexibility to allow the trapping of the photo-induced metastable state. Similar conclusions were obtained by Hashimoto and co-workers by studying the effect of the Na^+ content in the $Na_xCo_y[Fe(CN)_6][\square]_z{\cdot}nH_2O$ Prussian blue analogues from x = 0.07 to 0.94.[11] The infrared and UV-Vis spectra of the different compounds within this series showed that lower contents of sodium imposed a main Fe^{III}_{LS}–CN–Co^{II}_{HS} phase, while an increase of the Na^+ content rather stabilized the Fe^{II}_{LS}–CN–Co^{III}_{LS} configuration. For intermediate doping of Na^+, the average ligand field around the cobalt ion allows the occurrence of a thermal electron transfer, as well as a photo-induced ferrimagnetic state at low temperature. It should be noticed that these compounds were the first Prussian blue analogues exhibiting a thermal hysteresis associated with the thermally induced electron-transfer phenomenon (*i.e.* a first order phase transition). This phase transition was shifted towards high temperatures by increasing the amount of alkali metal ion. Additionally, it is worth mentioning that the relaxation of the thermally quenched state was studied in details for one related compound of this series, $Na_{0.4}Co_{1.4}[Fe(CN)_6]{\cdot}3.4H_2O$ (**7**).[40,41] This system was found to show a quasi-complete trapping of the high-temperature phase (when the sample was cooled down extremely fast), with a thermal decay of the quenched phase around 160 K. The mean-field analysis of the relaxation curves led to a relaxation time following a thermally activated behaviour (Arrhenius) with an energy barrier to electron transfer (Δ/k_B) of 3110(60) K and τ_0 = 6.7×10^{-7} s. This work represents the first evaluation of the relaxation time (τ) in a Fe/Co PBA, with a τ value of *ca.* 33 hours at 120 K.[40,41] Similarly, the relaxation properties of the photo-induced state from other systems of this family have also been explored. As an example, the lifetime of the photo-induced state in $Na_{0.6}Co_{1.21}[Fe(CN)_6]{\cdot}4.2H_2O$ was found to be about 3 hours at 120 K.[42]

2.3. Local magneto-structural characterization of Fe/Co PBAs: X-ray absorption spectroscopy and X-ray magnetic circular dichroism

One of the main issues faced during the study of Prussian blue analogues was the difficulty of establishing the local structure of the materials. Since PBAs are obtained as amorphous or weakly crystalline powders, information from X-ray diffraction are not very instructive. On the other hand, the combination of infrared and UV-Vis spectroscopies, together with powder X-ray diffraction, has been very useful for determining the main oxidation state of the metal ions in the PBAs, as well as the unit cell parameter. However as discussed before, the coordination sphere of each metal ion is the key to understand the electron transfer properties of these systems. Thus, fundamental information on their geometry and the nature of the coordinated atoms is required and therefore further analyses needs to be carried out. With these objectives, scientists have used X-ray absorption spectroscopy that offers the possibility to investigate the local structure/environment of a selected atom or metal ion. This technique is highly sensitive and provides information about the probed element's symmetry, nature of the coordinating atoms, metal–ligand distances but also its oxidation and spin states. In particular, Extended X-Ray-Absorption Fine-Structure (EXAFS) and X-Ray Absorption Near-Edge Structure (XANES) spectroscopies appeared to be the most efficient techniques for such characterizations. From EXAFS, the local geometries around the metal ions can be determined, while XANES is used to study their electronic structures. In that sense, Hashimoto and co-workers, as well as Cartier dit Moulin, Bleuzen, Verdaguer and co-workers, demonstrated the efficiency of both techniques to characterize the PBAs.[23,43,45–48] Several compounds have been studied by EXAFS and XANES (see Table 1), confirming and completing the information already obtained by the standard techniques mentioned above. As an example, a detailed comparison of six different compounds known to show different magnetic properties was carried out by Hashimoto and coworkers:[43] $Rb_{0.66}Co_{1.25}[Fe(CN)_6]{\cdot}4.3H_2O$ (**2**) and $K_{0.4}Co_{1.3}[Fe(CN)_6]{\cdot}5H_2O$ (**8**), which do not show any thermally-induced electron transfer but a ferrimagnetic ordered state upon irradiation; $Na_{0.4}Co_{1.3}[Fe(CN)_6]{\cdot}5H_2O$ (**9**) and $K_{0.4}Co_{1.3}[Fe(CN)_6]{\cdot}4.2H_2O$ (**10**), which display a thermally

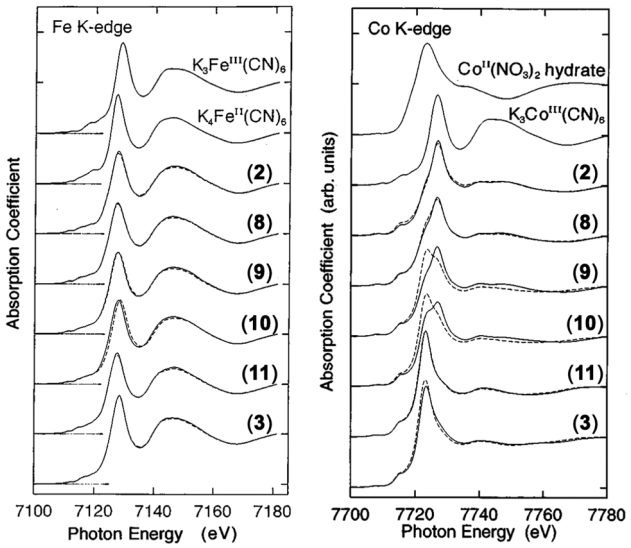

Fig. 3 Fe K-edge (left) and Co K-edge (right) XANES spectra for compounds **2**, **8**, **9**, **10**, **11** and **3** at 30 K (solid lines) and 296 K (dashed lines). Spectra for $K_3Fe^{III}(CN)_6$ and $K_4Fe^{II}(CN)_6$ (Fe K-edge) and for $K_3Co^{III}(CN)_6$ and $Co(NO_3)_2$ hydrate (Co K-edge) were added for comparison. Adapted with permission from ref. 43. Copyrighted by the American Physical Society.

induced electron transfer transition; and $Na_{1.4}Co_{1.3}[Fe(CN)_6]\cdot 5H_2O$ (**11**) and $Co_{1.5}[Fe(CN)_6]\cdot 6H_2O$ (**3**), for which the cobalt ion was assumed to be Co^{II}_{HS} at all temperatures. XANES spectra measured at the iron K edge (electronic transition from 1s to 4p orbitals; pre-edge from 1s to 3d orbitals) for all compounds and for the references, $K_3[Fe(CN)_6]$ and $K_4[Fe(CN)_6]$, confirmed the octahedral environment $Fe(CN)_6$ around the iron ion (Fig. 3, left). Nevertheless, a small edge energy shift to higher energy from Fe^{II}_{LS} to Fe^{III}_{LS} can be observed. Under this consideration, the spectra observed in compounds **2**, **8** and **11** suggested an oxidation state of Fe^{II}_{LS}, while in sample **3**, the iron site was closer to Fe^{III}_{LS}. Accordingly, the spectra for samples **9** and **10** showed a thermal dependence, since the spectra at 296 K (Fig. 3, left, dashed lines) and 30 K (Fig. 3, left, solid lines) did not perfectly overlap. However, XANES signatures at the Fe K-edge of both Fe^{II}_{LS} and Fe^{III}_{LS} states are very similar, and thus no quantitative analysis could be carried out. In contrast, marked differences can be observed in the Co K-edge XANES spectra as the results of the Co oxidation state change that imposes a different spin state (Fig. 3, right). Similarly to the Fe K-edge spectra, temperature dependence of the Co XANES signature was observed for **9** and **10** due to the $Co^{III}_{LS}/Co^{II}_{HS}$ conversion. In this case, clear differences can be observed in the spectra at high (Fig. 3, right, dashed lines) and low temperatures (Fig. 3, right, solid lines), with resemblances to the ones related to $Co^{II}(NO_3)_2$ and $K_3Co^{III}(CN)_6$, respectively. As expected, much smaller differences were found for compounds **2**, **3**, **8** and **11**.

Analyses of the EXAFS data were used to obtain specific structural information, such as the coordination geometry or interatomic distances around the metal ions. Interestingly, it was observed that Fe^{II}–C bond length distances are slightly shorter than in systems with Fe^{III}_{LS}–C bonds. This effect was attributed to the presence of an additional electron in the t_{2g} bonding orbital for Fe^{II}_{LS} site, that induces a slight shortening of the Fe–C bond compared to those involving Fe^{III}_{LS}. On the other hand, the EXAFS analysis for the Co^{II}_{HS}–N,O and Co^{III}_{LS}–N,O systems showed that the differences in the bond lengths were more similar to the ones found in Co/radical complexes showing valence tautomerism than in Co^{II} spin-crossover compounds. This study proved the change of Co valence within the studied materials and thus the electron transfer phenomena. In 1999, Hashimoto and co-workers went one step further and used XANES and EXAFS spectroscopies to study the local Fe and Co environments in the photo-excited state of $Na_{0.4}Co_{1.3}Fe(CN)_6\cdot 5H_2O$ (**9**).[47] This system was found to exhibit photo-induced electron transfer at low temperatures,[29] with a metastable state possessing lifetimes large enough around 40 K to be studied by these spectroscopic techniques. The features observed in the Co K-edge and Fe K-edge XANES spectra after irradiating the sample with visible light at 36 K were similar to those at 300 K, showing that the dominant Co and Fe species were in the oxidation state +2 and +3, respectively. After heating the sample to 150 K, the Co K-edge spectra turned back to the low temperature one (for Co^{III}_{LS}), implying that the trapped excited state was thermally relaxed to the ground state at this temperature. A further increase of the temperature until 300 K confirmed the presence of the Fe^{III}_{LS}–Co^{II}_{HS} phase and thus that the thermally induced electron-transfer was still present as for the non irradiated sample. By comparing the estimated Co^{III}/Co^{II} composition ratio, it was found that the amount of Co^{II} site was larger in the irradiated sample at 36 K than in the sample at 300 K, which evidenced the larger number of paramagnetic Fe^{III}_{LS}–Co^{II}_{HS} units in the photo-induced phase. Nevertheless, EXAFS spectroscopy showed that the local structure of the photo-induced state was very close to that of the high-temperature phase.

The influence of the alkali-metal ion in the thermally induced electron transfer phenomenon was also assessed by EXAFS spectroscopy. As an example, Bleuzen and co-workers studied $Cs_{0.24}Co_{1.38}[Fe(CN)_6]\cdot 5.5H_2O$ not only at the Fe and Co K-edges but also at the Cs L_3-edge.[44] The different EXAFS signals obtained at 300 and 20 K at Fe and Co K-edges were used to evidence the thermally induced electron transfer in this compound (see Table 1). On the other hand, the analysis of EXAFS data at the Cs L_3-edge demonstrated that at 300 K the Cs ion is not centred on the Td site of the Prussian blue network, inducing a bend of the Co–CN–Fe motifs. This structural feature, that implies a less efficient orbital overlap than in the linear conformation, imposes a weaker ligand field around the cobalt centre and thus stabilizes the Co^{II}_{HS} state. In contrast, the EXAFS experiments carried out at 20 K showed that the Cs ion is localized on the Td site, inducing a linear Co–CN–Fe conformation in its neighbourhood. The stronger orbital interaction promoted by such linearity produces a stronger ligand field around the cobalt ion, and thus stabilizes its Co^{III}_{LS} configuration. With these instructive results, the authors showed that the cobalt ions surrounding the Cs ions are the ones involved in the thermal electron transfer phenomenon,

thus proving the crucial role of the alkali metal ions in this process.

In order to study further the light-induced electron transfer process, Cartier dit Moulin, Bleuzen, Verdaguer and co-workers investigated the electronic and local structures of the ground and excited states of $Rb_{0.55}Co_{1.2}[Fe(CN)_6]\cdot 3.9H_2O$ (**5**) by XANES and EXAFS.[45] The comparison between the XANES spectra before and after irradiation below 30 K confirmed a decrease of the Co^{III}_{LS} and Fe^{II}_{LS} signals subsequent to the photo-induced conversion of some Co^{III}_{LS}–Fe^{II}_{LS} units into Co^{II}_{HS}–Fe^{III}_{LS} ones. However, it was estimated that about 46% of diamagnetic pairs remained unaffected by the irradiation. Therefore, two types of diamagnetic Co^{III}_{LS}–Fe^{II}_{LS} pairs were described: (i) active ones, which are located in a more flexible network (close to iron vacancies [□]) and can be easily converted into the paramagnetic Co^{II}_{HS}–Fe^{III}_{LS} configuration through light irradiation; and (ii) inactive ones, which are thought to have less or a lack of vacancies [□] in their neighbourhood, being trapped in a more rigid network that precludes the light-induced electron transfer. These two kinds of Fe^{II}_{LS}–CN–Co^{III}_{LS} moiety are naturally induced by the inhomogeneous repartition of the vacancies in the material, which implies a variety of environments around the cobalt centres (*vide supra*). Interestingly, the authors tried to de-excite the photo-induced state with a blue light as seen before by Hashimoto and co-workers for **1**.[22] Against expectations, the effect was found to be inversed, resulting in a further increase of the paramagnetic Co^{II}_{HS}–Fe^{III}_{LS} pair population. This observation illustrates the complexity of the materials with the presence of a distribution of geometries for the Fe^{II}_{LS}–CN–Co^{III}_{LS} moiety that display different photo-activities.[45] These EXAFS experiments also evidenced that the photo-induced electron-transfer was associated to a local structure rearrangement of the coordination sphere of the cobalt ions with a bond increase of about 0.17 Å. This large modification needs to be absorbed by the tridimensional network, and thus the efficiency of the photo-conversion of the Fe^{II}_{LS}–CN–Co^{III}_{LS} pairs depends on a subtle compromise between the number of diamagnetic pairs and vacancies [□] in the material.

One of the remaining questions concerning the photo-induced phase of Fe/Co PBAs was the nature of the exchange interaction between the magnetic Co^{II}_{HS} and Fe^{III}_{LS} sites. Even if it was assumed that antiferromagnetic interactions between the centres led to ferrimagnetic ground state,[22–24,31] no macroscopic characterization of this photo-induced metastable state could be carried out. The main difficulties were (i) to know the amount of the photo-transformed phase[45] (as the photo-conversion of the sample is never complete; *vide supra*), (ii) the possible partial relaxation to the diamagnetic state at low temperatures, and (iii) the fact that two configurations (antiferromagnetic $Co^{II}_{(HS,3/2)}$/$Fe^{III}_{(LS,1/2)}$ or ferromagnetic $Co^{II}_{(LS,1/2)}$/$Fe^{III}_{(LS,1/2)}$) cannot be easily discriminated as they generate a very similar resulting magnetic moment (around 2 μ_B).[46] However, Cartier dit Moulin, Bleuzen and co-workers showed that X-Ray Magnetic Circular Dichroism experiments (XMCD) were able to probe the relative orientation of the magnetic moments of the metal ions, and thus to determine the sign of the magnetic interaction. With this technique, they characterized the magnetic interaction within the photo-induced metastable state of compound **5** ($Rb_{0.55}Co_{1.2}[Fe(CN)_6]\cdot 3.9H_2O$),[46] that was compared to $K_{0.04}Co_{1.48}[Fe(CN)_6]\cdot 6.8H_2O$ (**4**), known to exhibit antiferromagnetic interactions between Co and Fe ions.[23] For both compounds, a weak dichroic signal was obtained at the Co and Fe K-edges, with positive and negative signs, respectively. Since the antiferromagnetic coupling between magnetic $Co^{II}_{(HS,3/2)}$ and $Fe^{III}_{(LS,1/2)}$ centres in **4** was shown already by macroscopic magnetization data, it was concluded that the inversion of dichroic signal from cobalt to iron was a local evidence of the antiferromagnetic interaction in **4**. With this assumption, and taking into account that the same XMCD signature was observed for **5**, the authors evidenced for the first time the ferrimagnetic ground state of the photo-induced phase in Fe/Co PBAs.

3. Introducing blocking ligands: reducing the dimensionality of the Prussian blue analogues

The previous section summarizes the research done in the past twenty years on tridimensional Fe/Co Prussian blue analogues, which display thermally and photo-induced electron transfer processes associated with optical and magnetic bistabilities between paramagnetic Fe^{III}_{LS}–CN–Co^{II}_{HS} and diamagnetic Fe^{II}_{LS}–CN–Co^{III}_{LS} configurations. In these systems, the amount of $[Fe(CN)_6]^{3-}$ vacancies can be modified through the nature and the quantity of the alkaline ions (Na^+, K^+, Rb^+, Cs^+…). These modifications highly influence the environment around the cobalt ion and its coordination sphere that is completed by water molecules. These chemical variations allow the change of the network flexibility, as well as the modification of the ligand field around the cobalt ion (and thus its local redox potential) influencing the electron transfer properties. Unfortunately, these vacancies and associated distortions of the network are inhomogeneously disseminated in the materials, resulting in a distribution of local environments around the cobalt ion. This feature promotes a distribution of electron transfer processes that coexist with inactive diamagnetic or paramagnetic Fe–CN–Co pairs. Moreover, the low solubility of these tridimensional materials precludes their manipulation and thus their easy shaping for technological applications. In that sense, materials with a lower structural dimensionality such as molecular, uni- or bi-dimensional systems, appeared to be an interesting strategy to face these challenges. These low dimensional systems allow not only a high control of the environment around the metal ions by a careful choice of the ligands, but also an increase of the solubility making easier the study of their structure and physico-chemical properties. These promising ideas encouraged several research groups in the world to design and search for low-dimensional Fe/Co cyanide complexes by using blocking ligands to limit the extension of the PBA framework. The most representative

examples of this trend of research are described in the following sections.

3.1. First evidence of an intramolecular electron transfer process in a discrete Fe/Co cyanide-based complex

Although some low-dimensional Fe/Co cyanide complexes were reported during the emergence of the Fe/Co Prussian blue networks, none of these examples showed evidence of a thermally or photo-induced electron transfer phenomena.[49–53] However in 2004, the seminal works of Dunbar, Achim and co-workers reported for the first time a cyanido-bridged Fe/Co molecule exhibiting a thermally induced metal-to-metal electron transfer.[54,55] By reacting $[Fe(CN)_6]^{3-}$ and $[Co(tmphen)_2]^{2+}$ (tmphen: 3,4,7,8-tetramethyl-1,10-phenanthroline), a pentanuclear complex, $\{[Co(tmphen)_2]_3[Fe(CN)_6]_2\}$ (**12**), was obtained (Fig. 4, top). This molecule exhibits a trigonal bipyramidal geometry, with three $[Co(tmphen)_2]^{2+}$ units forming the central equatorial plane and two $[Fe(CN)_6]^{3-}$ moieties completing the apical positions. While the Fe–C bonds in the crystal structures at low and high temperatures did not exhibit significant differences, a decrease of the Co–N distances (*ca.* 0.12–0.14 Å) was observed for two of the three cobalt ions when lowering from 220 to 110 K. These results suggest the presence of Co centres experiencing a conversion from a divalent high spin configuration (Co^{II}_{HS}) to a trivalent low-spin one (Co^{III}_{LS}). At the same time, Mössbauer spectroscopy confirmed the presence of only Fe^{III} sites at high temperatures, while features for both Fe^{II} and Fe^{III} centres, in an approximate 1 : 1 ratio, were observed at low temperature. From these observations, the authors concluded on the oxidation state of the five metal ions for the complex **12** as $[Co^{II}_3Fe^{III}_2]$ at high temperature, while they proposed two possibilities at low temperature: a $[Co^{II}_2Co^{III}Fe^{II}Fe^{III}]$ configuration with a statistical disorder of the Co^{III} and Fe^{II} centres on two different Co and Fe sites respectively, or a mixture of $[Co^{II}Co^{III}_2Fe^{II}_2]$ and $[Co^{II}_3Fe^{III}_2]$ species. The temperature dependence of the magnetic susceptibility of **12** revealed a χT value of 8.3 cm^3 K mol^{-1} above 270 K, confirming the presence of three Co^{II}_{HS} (S = 3/2) and two Fe^{III}_{LS} (S = 1/2) ions (Fig. 4, bottom, red crystals). When cooling the sample, the χT product decreased significantly to reach a value of 3.3 cm^3 K mol^{-1} at 2 K,[54] in agreement with the author's first hypothesis (*vide supra*) and a $[Co^{II}_2Co^{III}Fe^{II}Fe^{III}]$ state at low temperature. These results showed for the first time the possibility to obtain a metal-to-metal electron transfer within a discrete Fe/Co complex. It is worth mentioning that after a prolonged air exposure, this sample experienced a transformation from a red crystalline material to a blue powder due to water absorption. Mössbauer and magnetic susceptibility measurements of this new phase indicated the presence of a low temperature $[Co^{II}Co^{III}_2Fe^{II}_2]$ phase below 200 K. The gradual increase of the χT product above this temperature, together with the appearance of a small quadrupole doublet in the Mössbauer spectrum originated from a Fe^{III}_{LS} centre, supported an electron-transfer process from Fe^{II}_{LS} to Co^{III}_{LS} within the compound, suggesting the thermal population of a $[Co^{II}_3Fe^{III}_2]$ configuration (Fig. 4, bottom, blue solid). Interestingly, a third solid-state phase was obtained when the blue powder was exposed to high temperatures or vacuum, changing its colour to red. Mössbauer spectroscopy on this new phase revealed only the signature of Fe^{III}_{LS} centres independently of the temperature, and thus suggesting a stable $[Co^{II}_3Fe^{III}_2]$ configuration above 2 K. This hypothesis was confirmed by magnetic susceptibility measurements, which display only a smooth decrease attributed to the orbital contribution of both metal ions in the complex (Fig. 4, bottom, red solid). Even if compound **12** is not a molecular fragment of the original tridimensional Fe/Co Prussian blue analogue (*vide infra*, Section 3.2), this complex should be considered as the first discrete Fe/Co cyanide-based species exhibiting a thermally induced intramolecular electron transfer.

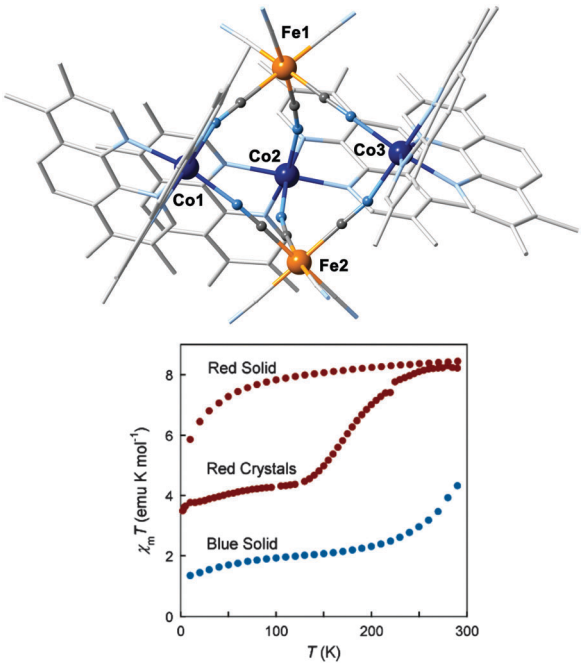

Fig. 4 (top) Representation of the molecular structure of $\{[Co(tmphen)_2]_3[Fe(CN)_6]_2\}$ (**12**) at T = 220 K. Hydrogen atoms are omitted for clarity. Fe, Co, N and C atoms are indicated in orange, dark blue, light blue and light grey, respectively. (bottom) χT *versus* T data of **12** at a constant magnetic field of 0.1 T for the three solid-state phases obtained (red crystals, red and blue powders). Reprinted with permission from ref. 55. Copyright 2005 American Chemical Society.

A few years later in 2011, the photomagnetic properties of **12** were reported by Dunbar, Clérac, Mathonière and co-workers by measuring the temperature dependence of the magnetic susceptibility of compound **12** after exposure to the humidity (blue powder phase) before and after irradiation.[56] As expected[54,55] the magnetic properties agreed with a $[Co^{II}Co^{III}_2Fe^{II}_2]$ configuration at low temperatures (*vide supra*) that appeared to be photo-active as indicated by a fast increase of the magnetic response after irradiation at 10 K with white light. This effect was attributed to a partial photo-conversion (about 30%) of the $[Co^{II}Co^{III}_2Fe^{II}_2]$ state to the $[Co^{II}_3Fe^{III}_2]$ one. The authors related the incomplete nature of the photomagnetic effect to the dark colour of the sample (which likely impeded the light penetration) or to the difficulty to access

to the $[Co^{II}_3Fe^{III}_2]$ configuration from the blue solid phase. Above 50 K, the photo-excited state relaxed to the thermodynamic $[Co^{II}Co^{III}_2Fe^{II}_2]$ phase, that reproducibly exhibits the same magnetic properties observed before irradiation.[56]

3.2. "Extracting" molecular units from the tridimensional Fe/Co Prussian blue analogue

3.2.1. The first step: an octanuclear cubane complex. The studies carried out by Dunbar *et al.* demonstrated for the first time the possibility of observing an electron transfer phenomenon within a molecular Fe/Co system. However some years later in 2008, the first molecular fragment of the tridimensional Fe/Co Prussian blue analogue was reported by Clérac, Mathonière, Holmes and co-workers. This complex, $\{[(pzTp)Fe^{III}(CN)_3]_4[Co^{II}(pz)_3CCH_2OH]_4\}[ClO_4]_4\cdot 13DMF\cdot 4H_2O$ (**13**, pzTp: tetrapyrazolylborate, $(pz)_3CCH_2OH$: 2,2,2,-tris(pyrazolyl)-ethanol), is an octanuclear species which truly represents the elementary unit of the 3D PBA network.[57] This cationic $[Fe_4Co_4]$ molecular cube was obtained by reacting $[NEt_4][(pzTp)Fe^{III}(CN)_3]$ with $Co(ClO_4)_2$ in DMF, with the subsequent addition of $(pz)_3CCH_2OH$ ligand. Earlier to this work, it is worth mentioning that this synthetic strategy using blocking/capping ligands had been successfully applied by Long,[58] Rauchfuss[59] and co-workers to obtain other molecular homo- and hetero-metallic cyanido-bridged cubes. In the case of complex **13**, both cobalt and iron centres are located at the corners of the molecular cube (Fig. 5, top) that is surrounded in the crystal packing by perchlorate anions and solvent molecules. Crystallographic studies at 260 and 90 K first evidenced the occurrence of an electron transfer phenomenon in this complex. At high temperatures, bond analysis and charge compensation indicated the presence of four Fe^{III}_{LS}–Co^{II}_{HS} pairs within the cube. In contrast, when this compound is cooled down to 90 K, the Co–N bond distances fall in the range expected for a Co^{III}_{LS} site (average value: 1.905(7) Å) suggesting the occurrence of a thermal electron transfer converting four Fe^{III}_{LS}–Co^{II}_{HS} pairs (observed at 260 K) in four Fe^{II}_{LS}–Co^{III}_{LS} pairs (at 90 K). Differential scanning calorimetry (DSC) revealed the presence of an endothermic peak at 255 K indicating the occurrence of a phase transition associated with the intramolecular electron transfer that was also studied by temperature dependent infrared (IR) and UV-Vis spectroscopies. The IR studies focussed on the ν_{CN} stretching mode that is a good internal probe of the bridging mode of the cyanide groups. The formation of Fe^{II}_{LS}–CN–Co^{III}_{LS} units in temperature was monitored by following the reversible shift of this IR band from high to lower energies when decreasing the temperature. Similar temperature studies were also performed analysing the UV-visible spectra, both in solution (CH_3CN) and in solid state.

The magnetic properties as a function of temperature and light irradiation were carried out to further study the physical properties of compound **13**. Magnetic susceptibility measurements revealed a constant χT product of 12.7 cm^3 K mol^{-1} from 300 to 265 K, in a good agreement with non interacting Fe^{III}_{LS} and Co^{II}_{HS} magnetic centres in a 4 : 4 ratio (Fig. 5, bottom). An abrupt and reproducible decrease of the χT value down to 0.57 cm^3 K mol^{-1} was observed when the sample was cooled

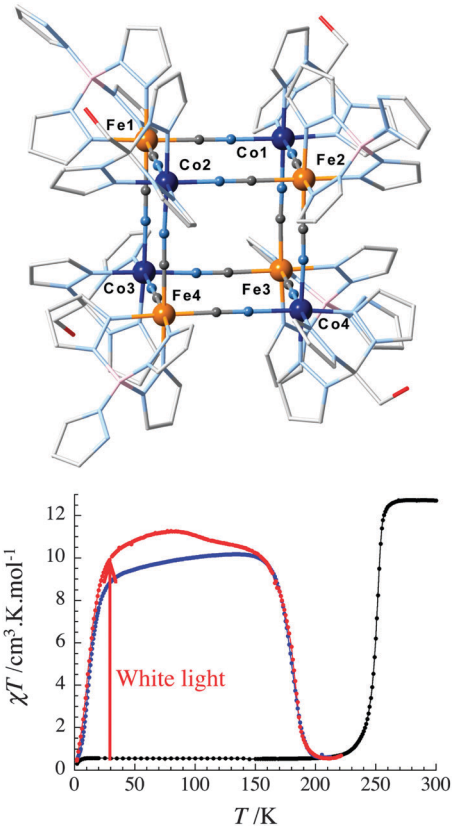

Fig. 5 (top) Representation of the molecular structure of $\{[(pzTp)Fe^{III}(CN)_3]_4[Co^{II}((pz)_3CCH_2OH)]_4\}[ClO_4]_4\cdot 13DMF\cdot 4H_2O$ (**13**) at T = 260 K. Hydrogen atoms, perchlorate and lattice-solvent molecules are omitted for clarity. Fe, Co, N, C, O and B atoms are indicated in orange, dark blue, light blue, light grey, red and pink, respectively. (bottom) χT *versus* T data of **13** at 0.4 K min^{-1} and a constant magnetic field of 1 T before (black dots) and after (red dots) white light irradiation, and after thermal quenching (blue dots). Reprinted with permission from ref. 57. Copyright 2008 American Chemical Society.

below 255 K, evidencing the intramolecular electron transfer from the paramagnetic $[Fe^{III}_{LS}Co^{II}_{HS}]_4$ configuration into the diamagnetic $[Fe^{II}_{LS}Co^{III}_{LS}]_4$ one. Moreover, the authors demonstrated that the high temperature $[Fe^{III}_{LS}Co^{II}_{HS}]_4$ phase can be thermally trapped by rapidly cooling the sample, or photogenerated at 30 K after 20 hours of white light irradiation. A gradual increase of the temperature (at 0.4 K min^{-1}) allowed the complete relaxation of the metastable state toward the thermodynamic $[Fe^{II}_{LS}Co^{III}_{LS}]_4$ phase at about 180 K. This remarkably high relaxation temperature clearly evidenced the long lifetime of the metastable state, which was further studied as a function of the temperature. For both thermally and photo-induced metastable states, the characteristic relaxation time (τ) followed the same Arrhenius law with an extremely large activation energy barrier of 4455 K and $\tau_0 = 2.6 \times 10^{-8}$ s. In comparison to tridimensional PBAs, 7 or $Na_{0.6}Co_{1.21}[Fe(CN)_6]\cdot 4.2H_2O$, which possess τ values at 120 K of *ca.* 33 or 3 hours respectively,[40–42] this $[Fe_4Co_4]$ molecular cube possesses an exceptionally long relaxation time estimated at 10 years at 120 K.[57]

3.2.2. Reducing to tetranuclear species: square complexes. The evaluation of the physical properties of compound **13** evidenced that (i) both photo- and thermally induced electron transfer properties of the tridimensional Fe/Co PBAs were able to be transferred into molecular species, and (ii) a diamagnetic molecular complex can be fully converted into a paramagnetic one through a photo-induced electron transfer. The next question in this field of research was obvious: is it possible to reduce the size of this photo-active molecular PBAs to even smaller systems than this cube complex? This question was answered first by isolating a "face" of this octanuclear Fe/Co cube using again the successful building block approach. In fact, this kind of square complex was already described by Oshio and co-workers in 2000 by bridging iron and cobalt metal ions through cyanide groups, and capping them using bpy ligand (bpy = 2,2′-bipyridine).[60] Nevertheless, the two reported heterometallic compounds exhibited $[Fe^{II}_{LS}Co^{III}_{LS}]_2$ or $[Fe^{II}_{LS}Co^{II}_{HS}]_2$ configurations, and no evidence of electron transfer was found. In contrast in 2010, Clérac, Mathonière, Holmes and co-workers showed the occurrence of a reversible thermally and light-induced electron transfer in the tetranuclear $[Fe_2Co_2]$ complex $\{[(Tp^*)Fe^{III}(CN)_3]_2[Co^{II}(bpy)_2]_2\}[OTf]_2\cdot 4DMF\cdot 2H_2O$ (**14**, Tp*: tris(3,5-dimethyl)pyrazolyl borate, OTf: trifluoromethanesulfonate).[61] This compound was obtained by treating $[NEt_4][(Tp^*)Fe(CN)_3]$ with $Co(OTf)_2$ and bpy in DMF. The crystal structure at 230 K evidenced $\{(bpy)_2Co\}$ and $\{(Tp^*)Fe\}$ moieties located alternatively at the square corners and linked by cyanide ligands to afford Fe–CN–Co edges (Fig. 6, top). This molecule exhibited a nearly planar geometry, with a slightly distorted $[Fe_2(\mu\text{-}CN)_4Co_2]$ square core. At this temperature, the Co–N bond distances revealed the Co^{II} high spin configuration, suggesting the formation of $[Fe^{III}_{LS}Co^{II}_{HS}]_2$ paramagnetic species by charge balance consideration. This high temperature configuration was further confirmed by IR spectroscopy and the corresponding ν_{CN} stretches for Fe^{III}_{LS}–CN–Co^{II}_{HS} units. When the spectra were recorded at 130 K, characteristic bands for diamagnetic Fe^{II}_{LS}–CN–Co^{III}_{LS} pairs were observed. It is important to mention that these thermal variations were perfectly reversible upon cycling the temperature of the sample. Similarly, optical properties (solid state UV-Vis spectroscopy and optical reflectivity) were also found to be temperature dependent. In particular, the optical reflectivity was recorded between 260 and 10 K, exhibiting an abrupt and hysteretic change of the absolute value between 200 and 160 K. Moreover, the reflectivity spectrum at 10 K after irradiating the sample for 4 hours was similar to the high temperature one, thus evidencing the photo-activity of the compound. This photo-generated state relaxed to the thermodynamic configuration around 130 K when the sample was heated. For a deeper analysis and the identification of the different phases, the observed thermally and light-induced electron transfer phenomena were studied by magnetic measurements (Fig. 6, bottom). At high temperature, the χT value of 6.8 cm^3 K mol^{-1} agreed well with the presence of two Fe^{III}_{LS} and two Co^{II}_{HS} magnetic centres. By decreasing the temperature, an abrupt decay of the χT product was observed around 168 K reaching 0.4 cm^3 K mol^{-1} at 120 K. This result confirmed the expected thermal electron transfer between Co^{II}_{HS} and Fe^{III}_{LS} leading to the conversion of paramagnetic $[Fe^{III}_{LS}Co^{II}_{HS}]$ pairs into diamagnetic $[Fe^{II}_{LS}Co^{III}_{LS}]$ ones. Upon increasing the temperature, the reversible phenomenon was observed at 186 K underlining a broad thermal hysteresis of 18 K (1 K min^{-1}) and thus the first order phase transition associated with the electron transfer process. This phase transition was further confirmed by the presence of enthalpic peaks in the DSC thermograms. The photomagnetic properties of **14** were also studied at 10 K by irradiation of the sample with white light. As anticipated from the reflectivity measurements, a sharp increase of the χT product was observed in agreement with the photo-generation of paramagnetic Fe^{III}_{LS}–CN–Co^{II}_{HS} pairs. This metastable $[Fe^{III}_{LS}Co^{II}_{HS}]_2$ state was also obtained by thermal quenching of the sample. Nevertheless, the lower χT values measured for the quenched phase demonstrate the higher efficiency of the light to generate this metastable paramagnetic phase. Both quenched and photo-induced metastable states were found to relax with relatively long characteristic times which follow an Arrhenius law with Δ/k_B = 2854 K and $\tau_0 = 9.1 \times 10^{-9}$ s. For comparison with the previous systems (*vide supra*), this $[Fe_2Co_2]$ molecular square possesses a relaxation time estimated at 3 minutes at 120 K.[61]

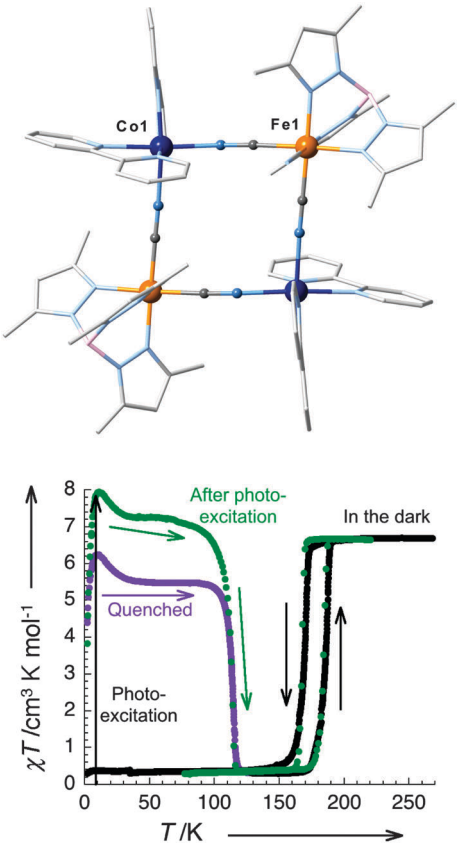

Fig. 6 (top) Representation of the molecular structure of $\{[(Tp^*)Fe^{III}(CN)_3]_2[Co^{II}(bpy)_2]_2\}[OTf]_2\cdot 4DMF\cdot 2H_2O$ (**14**) at T = 230 K. Hydrogen atoms, triflate and lattice-solvent molecules are omitted for clarity. Fe, Co, N, C, and B atoms are indicated in orange, dark blue, light blue, light grey, and pink, respectively. (bottom) χT *versus* T data of **14** at 0.4 K min^{-1} before (black dots, 0.1 T) and after (green dots, 1 T) white light irradiation, and after thermal quenching (purple dots, 0.1 T). Reprinted with permission from ref. 61. Copyright 2010 Wiley-VCH.

After the discovery of **14**, several other Fe/Co molecular square complexes featuring thermally and/or photo-induced electron transfer have been reported.[62] Using a similar building block approach, different groups have obtained these new square complexes by the modification of the ligands capping the metal centres or by looking at the influence of the counter-ion or the synthesis/crystallization solvent mixture. Indeed, the functionalization of the 2,2′-bipyridine ligand (bpy) has been one of the main approaches to develop new tetranuclear $[Fe_2Co_2]$ square compounds. For example, the addition of alkyl R groups on bpy (bpy^R) tunes the electronic properties of the final complex, but also its solubility. The first related complexes were reported by Oshio and co-workers who synthesized and studied $\{[(Tp^*)Fe^{III}(CN)_3]_2[Co^{II}(bpy)_2]_2\}[PF_6]_2\cdot 2MeOH$ (**15**) and $\{[(Tp^*)Fe^{III}(CN)_3]_2[Co^{II}(dtbbpy)_2]_2\}[PF_6]_2\cdot 2MeOH$ (**16**, dtbbpy: 4,4′-di-*tert*-butyl-2,2′-bipyridine).[63,64] The former analogue was found to exhibit a paramagnetic $[Fe^{III}_{LS}Co^{II}_{HS}]_2$ state independently of the temperature. The absence of electron-transfer properties was attributed by the authors to the lack of donating group on the bpy ligand, which results in an increase of the redox potential at the cobalt site. This hypothesis, that was proposed by comparing the redox properties of both **15** and **16** (*vide infra*),[64a] contrasts completely with the results observed for **14**,[61] which rather suggest a strong influence of the counter-ion within these systems and more generally the importance of the crystal packing on the electron transfer properties. Remarkably, complex **16** showed a two-step thermally induced electron transfer behaviour, with diamagnetic $[Fe^{II}_{LS}Co^{III}_{LS}]_2$ and paramagnetic $[Fe^{III}_{LS}Co^{II}_{HS}]_2$ configurations at low and high temperatures, respectively. In between at intermediate temperatures, the nature of the phase is still controversial. While infrared spectroscopy and X-ray diffraction studies suggest a 1 : 1 mixture of both $[Fe^{II}_{LS}Co^{III}_{LS}]_2$ and $[Fe^{III}_{LS}Co^{II}_{HS}]_2$ squares, DFT calculations support the stabilization of a one-electron transfer species with a $[Fe^{II}_{LS}Co^{III}_{LS}Fe^{III}_{LS}Co^{II}_{HS}]$ configuration.[64b] The photo-generation of the paramagnetic phase was successfully carried out by irradiating the compound with an 808 nm laser at 5 K. The light-induced metastable state was found to relax to the $[Fe^{II}_{LS}Co^{III}_{LS}]_2$ state around 80 K when increasing the temperature, as well as by irradiating the sample with green light (532 nm) at 5 K.[65] The same authors have also recently characterized compound **16** before and after irradiation using X-ray diffraction and X-ray absorption spectroscopy.[65,66] Interestingly, the X-ray beam itself was also found to produce the paramagnetic $[Fe^{III}_{LS}Co^{II}_{HS}]_2$ state, since accumulating XAS measurements on the diamagnetic $[Fe^{II}_{LS}Co^{III}_{LS}]_2$ state at 15 K induced gradual changes in the XAS spectra with time toward the one observed at high temperature.[66]

Another important result was reported by Oshio and co-workers, who used compound **16** to demonstrate for the first time the possibility of transferring the electron transfer phenomenon and the associated properties from solid state to solution.[64] When **16** was dissolved in butyronitrile, significant changes were observed in temperature by UV-Vis spectroscopy. Reducing the temperature, the intensity of the UV-Vis band associated with the $[Fe^{III}_{LS}Co^{II}_{HS}]_2$ state described a S-shape variation and the signature of the $[Fe^{II}_{LS}Co^{III}_{LS}]_2$ state was observed below 200 K. Remarkably, the thermal equilibrium between the two $[Fe^{II}_{LS}Co^{III}_{LS}]_2$ and $[Fe^{III}_{LS}Co^{II}_{HS}]_2$ states and their respective populations in solution were determined for the first time in temperature by UV-Vis spectroscopy. It is also important to mention that the intermediate state detected in solid state was absent in solution likely due to the lack of intermolecular interactions in solution.[64] Furthermore, UV-Vis spectroscopy was also used to monitor the electron transfer process upon addition of trifluoroacetic acid at fixed temperature. This remarkable result demonstrated for the first time the possibility of inducing an electron transfer in these molecular Fe/Co PBAs by protonation. The same authors also explored the possibility of changing the ligand capping the iron centre by using the Tp ligand (Tp: hydrotris(pyrazol-1-yl)borate) to synthesize the related compound $\{[(Tp)Fe^{III}(CN)_3]_2[Co^{II}(dtbbpy)_2]_2\}[PF_6]_2\cdot 4H_2O$ (**17**).[64] The absence of methyl groups on the Tp ligand stabilizes the Fe^{II} low spin state, thus leading to a diamagnetic $[Fe^{II}_{LS}Co^{III}_{LS}]_2$ electronic configuration for **17** in the whole temperature range. The good solubility of these $[Fe_2Co_2]$ systems permitted the study of their electron transfer by electrochemical measurements. Four redox processes attributed to the $[Fe_2Co_2]^{2+}$ moiety were observed by cyclic voltammetry experiments permitting (i) the simple comparison of the redox potentials of each metal centre for complexes **15**, **16** and **17**, and (ii) to probe the influence of the ligand functionalization by alkyl groups. The authors concluded that the addition of electron donating groups on the bpy and Tp* ligand offers a control of the redox potential at the Co and Fe sites, respectively, allowing the stabilisation of a thermally induced electron transfer phenomenon in **16**.

The influence of the bpy functionalization was also studied by Clérac, Mathonière, and co-workers in particular with complex **18**, $\{[(Tp^*)Fe^{III}(CN)_3]_2[Co^{II}(bpy^{Me})_2]_2\}[OTf]_2\cdot DMF\cdot H_2O$, for which the bpy ligand of complex **14** is replaced by bpy^{Me} (bpy^{Me}: 4,4′-dimethyl-2,2′-bipyridine).[67] This simple modification influenced dramatically the thermally induced electron transfer mechanism and the associated properties. While complex **14** exhibited a first order transition with a significant thermal hysteresis associated with the electron transfer process (*vide supra*; Fig. 6), a thermal conversion (*i.e.* a thermal equilibrium between the two $[Fe^{II}_{LS}Co^{III}_{LS}]_2$ and $[Fe^{III}_{LS}Co^{II}_{HS}]_2$ states) was observed for **18**. Similarly to spin-crossover systems, the electron transfer transition in **14** is converted in an electron transfer conversion in **18** by decreasing the elastic interactions between the molecules (*i.e.* decreasing the cooperativity) thanks to weaker π–π interactions between bpy^{Me} moieties in **18** than between bpy ligands in **14**.[67]

Combined UV-Vis spectroscopy and magnetic measurements of **14** and **18** in the different solvents were used to confirm that the occurrence of the intramolecular electron transfer was preserved in solution.[67] While the electron transfer process was detected only in methanol and acetonitrile for **14**, the physical properties of **18** were transferred to dilute solutions using a larger number of solvents. Interestingly, the thermally induced electron transfer conversion was found to be

strongly influenced by the nature of the used solvent. For example, a shift of about 60 K was observed when comparing $T_{1/2}$ (temperature where the ratio between the paramagnetic and diamagnetic configurations is 1 : 1) for **18** in CH_3OH (240 K) and CH_2Cl_2 (180 K). A general tendency showed that $T_{1/2}$ values increased with the solvent polarity, allowing a fine tuning of the electron transfer properties simply by a judicious choice of the solvent or adjusting the composition of a solvent mixture. For comparison, the authors also reported the solution properties of the related compound **19**, $\{[(Tp^*)Fe^{III}(CN)_3]_2[Co^{II}(DMF)_4]_2\}[OTf]_2\cdot 2DMF$, possessing cobalt ions capped by only coordinating DMF molecules and not bpy type ligands like in the analogues described above.[61,67,68] In this case, the complex stays paramagnetic in solid state[68] but also in all the solvents tested,[67] confirming the influence of the ligand environment on the redox potential of the Co site and thus the occurrence of an intramolecular electron transfer process. Recently, Oshio and co-workers obtained a similar complex $\{[(Tp^*)Fe^{III}(CN)_3]_2[Co^{II}(dmbpy)_2]_2\}[PF_6]_2\cdot 4MeCN$ (**20**, dmbpy: 5,5′-dimethyl-2,2′-bipyridine), by changing the position of the methyl group on the bpy ligand in comparison to complex **18**.[69] Like for **19**, X-ray diffraction and magnetic measurements in the solid state evidenced that **20** is stabilised in its paramagnetic $[Fe^{III}_{LS}Co^{II}_{HS}]_2$ configuration independently of the temperature. These results highlight how sensitive is the electron transfer process for these $[Fe_2Co_2]$ square complexes in the solid state and solutions, regarding the functionalization of the bpy ligand, as well as the choice of the counter-anions and the solvent molecules surrounding the complex.[60–69] The effect of the crystallisation solvent molecules was also illustrated by the appearance of both thermally and photo-induced electron transfer phenomena when **20** is desolvated.[69]

The influence of the ancillary ligands and the effect of the intermolecular interactions within these kinds of Fe/Co molecular squares were also recently studied by Holmes, Clérac, Mathonière and co-workers.[70] Two new complexes of this family, $\{[(Tp^{Me})Fe^{III}(CN)_3]_2[Co^{II}(bpy)_2]_2\}[(Tp^{Me})Fe^{III}(CN)_3]_2\cdot 12H_2O$ (**21**, Tp^{Me}: hydrotris(3-methylpyrazol-1-yl)borate) and $\{[(Tp^{Me})Fe^{III}(CN)_3]_2[Co^{II}(bpy)_2]_2\}[BPh_4]_2\cdot 6MeCN$ (**22**) were synthesized using $[NEt_4][(Tp^{Me})Fe^{III}(CN)_3]\cdot 9H_2O$ as a new iron building block. As their analogues, these $[Fe_2Co_2]$ systems show thermally and photo-induced electron transfer properties with a metastable paramagnetic state relaxing at 90 K and 120 K for **21** and **22**, respectively. The obtained $T_{1/2}$ values were 244 K for **21**, and 230 K for **22**. These values are higher than those observed for the related Tp*-based complexes (*i.e.*, 177 K for **14**, 174 K for **18**), demonstrating that the weaker σ donor character of the Tp^{Me} ligand stabilizes the low spin state of the Fe^{II} sites. This conclusion is corroborated by the properties of the related Tp-based complexes such as **17** (*vide supra*), which is diamagnetic due to an even weaker σ donor character of Fe capping ligand.[64] With this study, the authors demonstrated how the functionalization of the Tp ligand can also tune the electron transfer properties of the Fe/Co molecular squares. In contrast, no clear influence on $T_{1/2}$ was observed from the different intermolecular interactions detected in **21** and **22**. On the other hand, Li and co-workers synthesized and studied another example of a Fe/Co molecular square using the Tp ligand to chelate the iron sites and 4,4′-bis(ethoxycarbonyl)-2,2′-bipyridine (4,4′-bcbpy) as capping ligand for the cobalt centres: $\{[(Tp)Fe(CN)_3]_2[Co(4,4'\text{-bcbpy})_2]_2\}[ClO_4]_2\cdot 2MeOH$ (**23**·2MeOH).[71a] Accordingly, only the diamagnetic $[Fe^{II}_{LS}Co^{III}_{LS}]_2$ configuration was observed up to 300 K for **23**·2MeOH. However when the methanol molecules were removed from the lattice, complex **23** exhibited an incomplete thermally induced electron transfer to the paramagnetic $[Fe^{III}_{LS}Co^{II}_{HS}]_2$ state around 200 K. The authors attributed this effect to the loss of the hydrogen bonding network present between these molecular squares that is supposed to induce a negative shift of the redox potentials of the iron ions, thus promoting the electron transfer.[71a] Under external pressure (up to 8.35 kbar), the $T_{1/2}$ value increased slightly and the electron transfer process became almost complete. Remarkably when the crystals of **23** were soaked in methanol, the diamagnetic state was fully recovered, and this "crystal-to-crystal" transformation was found to be reversible. Interestingly, the same group recently published a related compound featuring similar ligands for both metal centres: $\{[(MeTp)Fe(CN)_3]_2[Co(4,4'\text{-bmbpy})_2]_2\}[PF_6]_2\cdot 2MeOH$ (**24**·2MeOH, MeTp: methyltris(pyrazolyl)borate, 4,4′-bmbpy: 4,4′-bis(methoxycarbonyl)-2,2′-bipyridine).[71b] While the metal ion precursors exhibit similar redox potentials to the ones in **23**·2MeOH, both thermal and photo-induced electron transfer processes were observed for compound **24**·2MeOH. The authors justified these contrasted behaviours by the significant distortion of the molecular square's core and the highly bent Co–N–C angles in **24**·2MeOH, which induce a decrease of the characteristic temperature of the electron transfer process.[71b] In this respect, Li's work introduces the influence of the square distortion and demonstrates once more the importance of the lattice environment in the electron transfer properties of these $[Fe_2Co_2]$ compounds.

Lescouëzec and co-workers also reported a Fe/Co cyanido-based square complex using the pzTp iron derivative and the bis(1-methylimidazol-2-yl)ketone (bik) ligand to coordinate at the cobalt centres: $\{[(pzTp)Fe(CN)_3]_2[Co(bik)_2]_2\}[ClO_4]_2\cdot 2H_2O$ (**25**).[72] While the magnetic measurements clearly indicates the diamagnetic nature of **25** between 2 and 300 K, the irradiation of the $[Fe^{II}_{LS}Co^{III}_{LS}]_2$ state (with white light at 20 K) led to a photo-induced electron transfer engendering paramagnetic $[Fe^{III}_{LS}Co^{II}_{HS}]_2$ species. In 2013, the same authors demonstrated that this metastable paramagnetic state in **25** could also be photo-generated using laser sources, with a high efficiency at 808 nm.[73] Interestingly, this photo-excited state was found to photo-relax to the diamagnetic one after irradiation at 532 nm, showing for the first time a bidirectional photomagnetic effect for a Fe/Co molecular PBA at a fixed temperature.

For comparison, the previously discussed $[Fe_2Co_2]$ systems are gathered in Table 2, mentioning the ligands occupying the iron (L_{Fe}) and cobalt (L_{Co}) coordination spheres, the used anion, the state of the compound for the study, the temperature at which the thermally induced electron transfer occurs and the temperature at which the system relaxes after a photo-induced electron transfer.

3.2.3. The smallest unit: a dinuclear complex. In the previous sections, we reviewed almost chronologically the

Table 2 Characteristics of the $\{[(L_{Fe})Fe^{III}(CN)_3]_2[Co^{II}(L_{Co})_n]_2\}[X]_2$ molecular squares described in the text

Compound	L_{Fe}	L_{Co}	Anion	$T_{1/2}$[b] (K) of the ET or magnetic state	T_{relax} (K) of the photo-induced state	State studied	Ref.
14	Tp*	bpy	OTf^-	168/186	120	Solid/solution	61 and 67
15	Tp*	bpy	PF_6^-	Paramagnetic	—	Solid	64
16	Tp*	dtbbpy	PF_6^-	275 and 310 (two steps)	80	Solid/solution	63 and 64
17	Tp	dtbbpy	PF_6^-	Diamagnetic	—	Solid/solution	64
18	Tp*	bpy^{Me}	OTf^-	174	120	Solid/solution	67
19	Tp*	$(DMF)_4$	OTf^-	Paramagnetic	—	Solid/solution	67
20[a]	Tp*	dmbpy	PF_6^-	240	100	Solid	69
21	Tp^{Me}	bpy	$[(Tp^{Me})Fe(CN)_3]^-$	244	100	Solid	70
22	Tp^{Me}	bpy	BPh_4^-	230	120	Solid	70
23[a]	Tp	4,4′-bcbpy	ClO_4^-	120	—	Solid	71*a*
24	MeTp	4,4′-bmbpy	PF_6^-	177/184	100	Solid	71*b*
25	pzTp	bik	ClO_4^-	Diamagnetic	100	Solid	72 and 73

[a] Data obtained from the desolvated form of the compound. [b] Temperature where the ratio between the paramagnetic and diamagnetic configurations is 1 : 1.

switchable Fe/Co Prussian blue networks and how their thermally and photo-induced electron transfer properties have been implemented in molecular objects, decreasing the nuclearity from an octanuclear cube, pentanuclear complexes to a tetranuclear square. The next obvious episode of this scientific adventure was naturally pointing toward the design of a simple dinuclear [FeCo] complex with electron transfer properties. Indeed, many dinuclear Fe/Co molecular complexes were reported in the literature by Bernhardt and co-workers.[49,51,74] Most of these complexes were obtained in a diamagnetic $[Fe^{II}_{LS}Co^{III}_{LS}]$ configuration, and none showed a thermally or photo-induced electron transfer phenomena. Only in 2005, Bernhardt, Hauser and co-workers studied by visible pump–probe spectroscopy the short-lived metal-to-metal electron transfer excited states of some of these dinuclear compounds.[75] By studying $[Fe^{II}_{LS}Co^{III}_{LS}]$ complexes, the authors were able to detect two different excited states with $[Fe^{III}_{LS}Co^{II}_{LS}]$ and $[Fe^{III}_{LS}Co^{II}_{HS}]$ configurations depending on the experimental time scale and pulse-width. While the former de-excited very fast (picosecond time scale), the back-electron transfer from the latter was found to be slower due to the required spin rearrangement and Co–N bond changes. Thus, the results obtained in this study provided a significant evidence towards the viability of the proposed CTIST mechanism.[11] Nevertheless, it was only in 2013 that the first dinuclear Fe/Co complex exhibiting electron transfer phenomena was finally synthesized and studied.[76] By using $PY5Me_2$ (2,6-bis(1,1-di(pyridine-2-yl)-ethyl)pyridine) and bbp^{2-} (2,6-bis(benzimidazol-2-yl)pyridine) as capping ligands, Clérac, Mathonière and co-workers obtained a new dinuclear Fe/Co complex, $[(bbp)Fe(CN)_3Co(PY5Me_2)]\cdot 2.5CH_3OH$ (**26**).[76] The bulky $PY5Me_2$ ligand around the cobalt precursor, $[Co(PY5Me_2)(OH_2)]^{2+}$, allowed only one accessible position in the Co coordination sphere for a cyanide ligand of the iron partner, $[Fe(bpp)(CN)_3]^{2-}$ thus stabilizing a dinuclear species in stoichiometric conditions (Fig. 7, top). At 370 K, the Co–N and Fe–C bond distances agreed well with Co^{II}_{HS} and Fe^{III}_{LS} sites, evidencing the paramagnetic $[Fe^{III}_{LS}Co^{II}_{HS}]$ state of the molecular pair. Magnetic susceptibility measurements revealed a gradual decrease of the χT value from high to low temperatures. While the high temperature χT value was in concordance with the paramagnetic $[Fe^{III}_{LS}Co^{II}_{HS}]$ configuration, also established by X-ray diffraction, the value found at lower temperatures was incompatible with a diamagnetic $[Fe^{II}_{LS}Co^{III}_{LS}]$ pair. In contrast, single-crystal X-ray diffraction, ^{57}Fe Mössbauer and magnetic studies revealed for the first time the presence of a different paramagnetic ground state with a $[Fe^{III}_{LS}Co^{II}_{LS}]$ configuration that was previously identified using visible pump–probe spectroscopy as an excited state in the dinuclear systems reported by Bernhardt, Hauser and co-workers.[75]

Unexpectedly, **26** exhibits a spin-crossover process occurring at the cobalt site in the solid state.[76] Nevertheless when **26** was studied in solution, different physical properties were observed. DMSO solutions of **26** were studied by magnetic susceptibility measurements to show that the spin-crossover behaviour is lost and only the paramagnetic $[Fe^{III}_{LS}Co^{II}_{HS}]$ configuration is observed above 1.8 K. However, when DMSO solutions were treated with an acid (trifluoroacetic or trifluoromethanesulfonic acids), their colour changed from dark green to purple. This proton-induced evolution was proven to be associated with a change of the [FeCo] pair electronic configuration by UV-vis spectroscopy, following the concomitant disappearance of the ligand-to-metal charge transfer band and the appearance of the metal-to-ligand charge transfer absorption centred on the iron moiety upon acid addition (Fig. 7, bottom). Moreover, the ^{1}H NMR spectra measured before and after acidifying the solution demonstrated the conversion of the paramagnetic $[Fe^{III}_{LS}Co^{II}_{HS}]$ complexes into diamagnetic species which can only be $[Fe^{II}_{LS}Co^{III}_{LS}]$ pairs. Using combined cyclic voltammetry and UV-vis spectroscopy on **26** and its molecular precursors, it was shown that the proton addition only affects the iron redox properties, shifting its potential toward the unaffected Co one and thus promoting the electron transfer mechanism. By crystallizing the iron precursor after protonation ($[Fe(H_2bbp)(CN)_3]\cdot 2H_2O$), the authors revealed that added protons were indeed doubly protonating the bpp ligand affecting only the redox properties of the Fe site. Remarkably, complex **26** is the first dinuclear [FeCo] PBA to exhibit a metal-to-metal electron transfer, and this process is not triggered by temperature or light but by protonation.[76]

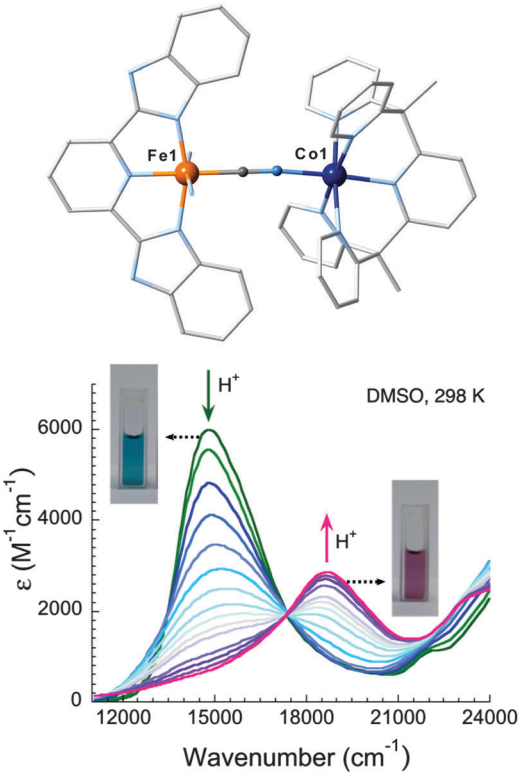

Fig. 7 (top) Representation of the molecular structure of [(bbp)Fe(CN)$_3$Co(PY5Me$_2$)]·2.5MeOH (**26**) at T = 370 K. Hydrogen atoms and lattice-solvent molecules are omitted for clarity. Fe, Co, N and C atoms are indicated in orange, dark blue, light blue and light grey, respectively. (bottom) Evolution of the UV-Vis spectra upon TFA (TFA: trifluoroacetic acid) addition to a solution of **26** in DMSO, showing the colour change from dark green (paramagnetic, [$Fe^{III}_{LS}Co^{II}_{HS}$]) to purple (diamagnetic, [$Fe^{II}_{LS}Co^{III}_{LS}$]). Reproduced from ref. 76 with permission from The Royal Society of Chemistry.

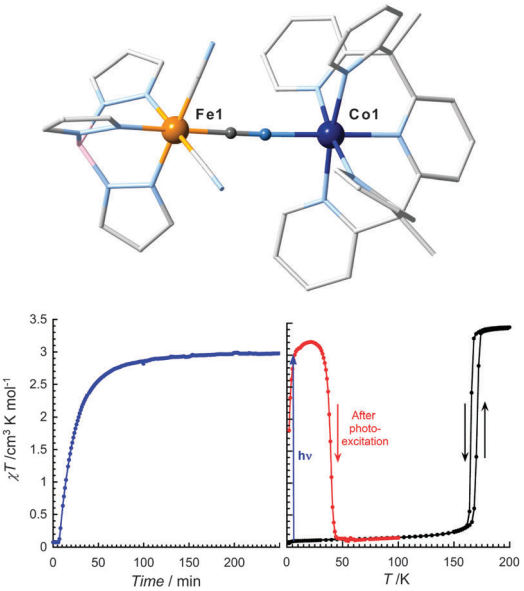

Fig. 8 (top) Representation of the molecular structure of [(Tp)Fe(CN)$_3$Co(PY5Me$_2$)](OTf)·2DMF (**27**·2DMF) at T = 180 K. Hydrogen atoms, triflate and lattice-solvent molecules are omitted for clarity. Fe, Co, N and C atoms are indicated in orange, dark blue, light blue and light grey, respectively. (bottom) χT *versus* time (blue circles) of the desolvated compound, **27**, at 1 T and 10 K under white light irradiation (3 mW cm^{-2}), and χT *versus* temperature before (black dots) and after (red dots) white light irradiation with a sweep rate of 0.4 K min^{-1}. Reprinted with permission from ref. 77. Copyright 2014 American Chemical Society.

The detailed study of the redox properties of **26** under protonation[76] was the key to obtain the first dinuclear Fe/Co complex exhibiting a thermally and light-induced electron transfer in the solid state. Clérac, Mathonière, Li and co-workers[77] replaced the $[Fe(bbp)(CN)_3]^{2-}$ building-block used in the synthesis of **26** by the $[(Tp)Fe^{III}(CN)_3]^-$ precursor that displays a redox potential in between those of $[Fe(bbp)(CN)_3]^{2-}$ and $[Fe(H_2bbp)(CN)_3]$, which combined with $[Co(PY5Me_2)]^{2+}$ afforded paramagnetic and diamagnetic dinuclear species respectively (*vide supra*).[76] This rational synthetic strategy successfully affords [(Tp)Fe(CN)$_3$Co(PY5Me$_2$)][OTf]·2DMF, (**27**·2DMF, Fig. 8, top) for which magnetic susceptibility and X-ray diffraction measurements demonstrated the presence of a partial (50%) thermally induced electron transfer in the solid state at 165 K. When **27**·2DMF was treated at high temperature and under vacuum, a quasi-complete electron transfer transition was observed at 170 K exhibiting a thermal hysteresis of about 5 K (with a sweep rate of 0.4 K min^{-1}; Fig. 8, bottom). As shown by IR spectroscopy, the heating/vacuum treatment of **27**·2DMF leads to a complete removal of the interstitial DMF molecules highlighting the crucial influence of the crystal packing on the electron transfer phenomenon. Solid-state optical reflectivity measurements and photomagnetic studies showed that the paramagnetic [$Fe^{III}_{LS}Co^{II}_{HS}$] configuration can be photo-induced at 10 K with a white light irradiation of the diamagnetic sample. This metastable phase relaxes to the thermodynamic [$Fe^{II}_{LS}Co^{III}_{LS}$] state after heating above 45 K (with a sweep rate of 0.4 K min^{-1}; Fig. 8, bottom). It is worth mentioning that this temperature is the lowest relaxation temperature observed for any molecular PBAs and it seems to decrease with the miniaturization of the complex. From these results, complex **27** can be then considered as the first dinuclear Fe/Co PBA exhibiting both thermally and photo-induced electron transfer processes in the solid state.[77]

3.3. Other molecular Fe/Co cyanide-based complexes with high nuclearity and electron transfer properties

The molecular systems reviewed in Section 3.2 feature the characteristics of ''extracted'' molecular units (cube, square and pair) from the tridimensional Fe/Co Prussian blue networks.[57,60–67,69–73,76,77] These different Fe/Co cyanide-based complexes illustrate beautifully how, nowadays, coordination chemistry is able to design step-by-step model systems with targeted physical properties from bulk materials. Since the molecular origin of the metal-to-metal electron transfer in Fe/Co PBAs was clearly elucidated by the dinuclear complexes,[76,77] a few other discrete polynuclear Fe/Co compounds exhibiting similar properties have been reported, even if they are not strictly a fragment of the 3D PBA network. In that sense, the pentanuclear

complex **12**, described in Section 3.1, should be considered as the first example of this subgroup.

Oshio and co-workers reported a tetradecanuclear $[Fe_8Co_6]$ complex $[Fe_8Co_6(\mu\text{-}CN)_{14}(CN)_{10}(Tp)_8(HL)_{10}(CH_3CN)_2][PF_6]_4\cdot 14CH_3CN\cdot 5H_2O$ (**28**·$14CH_3CN\cdot 5H_2O$, HL: 3-(2-pyridyl)-5-[4-(diphenylamino)phenyl]-1*H*-pyrazole),[78] by reacting $[NBu_4][(Tp)Fe(CN)_3]$ with $Co(BF_4)_2\cdot 6H_2O$ in the presence of HL and $[NBu_4]PF_6$. A crown-like complex was obtained, exhibiting a twelve-membered ring with alternated Fe and Co metal ions decorated with two dangling $[(Tp)Fe(CN)_3]^-$ moieties. Independently of the temperature, coordination bond lengths, magnetic measurements and Mössbauer spectroscopy revealed the paramagnetic $[(Fe^{III}_{LS})_8(Co^{II}_{HS})_6]$ configuration of **28**·$14CH_3CN\cdot 5H_2O$. However, when this compound was left at ambient temperature for several days, the magnetic properties changed drastically. Elemental analysis and TGA data established the total loss of the acetonitrile solvated molecules leading to formulate this compound as **28**·$5H_2O$. In this "aged" sample, a decrease of the χT product was observed from 250 to 150 K before levelling to a value of about 9.4 cm^3 K mol^{-1}. From these magnetic measurements, the authors concluded to the presence of a $[(Fe^{III}_{LS})_5(Fe^{II}_{LS})_3(Co^{II}_{HS})_3(Co^{III}_{LS})_3]$ configuration below 150 K in **28**·$5H_2O$. This low temperature phase was stabilized by a Co^{II} to Fe^{III} electron transfer in three Fe^{III}–CN–Co^{II} pairs from the high temperature $[(Fe^{III}_{LS})_8(Co^{II}_{HS})_6]$ state. Remarkably, this compound in its $[(Fe^{III}_{LS})_5(Fe^{II}_{LS})_3(Co^{II}_{HS})_3(Co^{III}_{LS})_3]$ configuration at 20 K was efficiently converted (at about 76%) in its fully paramagnetic $[(Fe^{III}_{LS})_8(Co^{II}_{HS})_6]$ state using laser irradiations (at 405 or 808 nm). Increasing the temperature, the photo-generated phase relaxed to its thermodynamic state above 150 K.[78]

Recently, the same group synthesized a new decanuclear Fe/Co complex containing six cobalt ions and four iron centres: $[NEt_4]_2\{[Co(L^R)]_6[Fe(CN)_6]_4\}[BF_4]\cdot 17CH_3OH\cdot 12H_2O$ (**29**, Fig. 9 top).[79] For its synthesis, the authors used the L^R ligand that was obtained *in situ* by reacting 2-pyridinecarbaldehyde and *R*-(+)-phenylethylamine, together with the metal ion precursors ($Co(BF_4)_2\cdot 6H_2O$ and $[NEt_4]_3[Fe(CN)_6]$). This serendipitous synthetic strategy led to a cage-type species, featuring six $[Co(L^R)_2]$ and four hexacyanoferrate units, encapsulating one tetraethylammonium cation (Fig. 9, top). Structural studies and Mössbauer spectroscopy evidenced the presence of a thermally induced electron transfer in **29** from a $[(Co^{II}_{HS})_5Co^{III}_{LS}(Fe^{II}_{LS})_2(Fe^{III}_{LS})_2]$ configuration at high temperatures to a $[(Co^{II}_{HS})_3(Co^{III}_{LS})_3(Fe^{II}_{LS})_4]$ state at 100 K. This conclusion was corroborated by magnetic susceptibility studies (Fig. 9, bottom) which detected a characteristic thermal variation of the χT product from 12.4 cm^3 K mol^{-1} at 300 K (close to the expected value for five Co^{II}_{HS} and two Fe^{III}_{LS} centres) down to 6.8 cm^3 K mol^{-1} below 180 K (in agreement with the value expected for three Co^{II}_{HS} ions) clearly associated with the metal-to-metal electron transfer process. As already observed for other compounds of this family, the desolvated version of **29** led to different physical properties with, in this case, a loss of the thermally induced electron transfer.[79]

3.4. Multifunctional molecular Fe/Co cyanide-based complexes with electron transfer properties

One of the most ambitious goals when synthesizing molecular cyanido-bridged Fe/Co complexes is to obtain multifunctional materials with a combination of the electron transfer behaviour and another physical property. A remarkable example was reported by Oshio and co-workers in a complex showing Single-Molecule Magnet (SMM)[80] properties due to a light-induced electron transfer.[81] By reacting $[NBu_4][(pzTp)Fe(CN)_3]$ with $Co(OTf)_2\cdot 6H_2O$ and bimpy in 1-PrOH, the authors obtained an hexanuclear compound: $[Co_2Fe_4(bimpy)_2(CN)_6(\mu\text{-}CN)_6(pzTp)_4]\cdot 2(1\text{-}PrOH)\cdot 4H_2O$ (**30**, bimpy: 2,6-bis(benzimidazol-2-yl)pyridine). The complex exhibited a square core composed of two $[(pzTp)Fe(\mu\text{-}CN)_2(CN)]^-$ and two $[Co(bimpy)]^{2+}$ moieties decorated by two more $[(pzTp)Fe(CN)_2(\mu\text{-}CN)]^-$ modules linked to each cobalt centre (Fig. 10, top). By using the tridentate bimpy ligand, one position around the cobalt ion coordination sphere is left available consenting the targeted square motif to be kept and at the same time allowing the coordination of the two additional iron units. As for the previous complexes, the high and low temperature configurations were assessed by single-crystal X-ray diffraction and ^{57}Fe Mössbauer spectroscopy. While cobalt and iron sites at 250 K were found to be Co^{II}_{HS} and Fe^{III}_{LS}, respectively, the study carried out at 100 K revealed a Co^{III}_{LS} configuration for the two cobalt centres, and two different oxidation/spin states for the

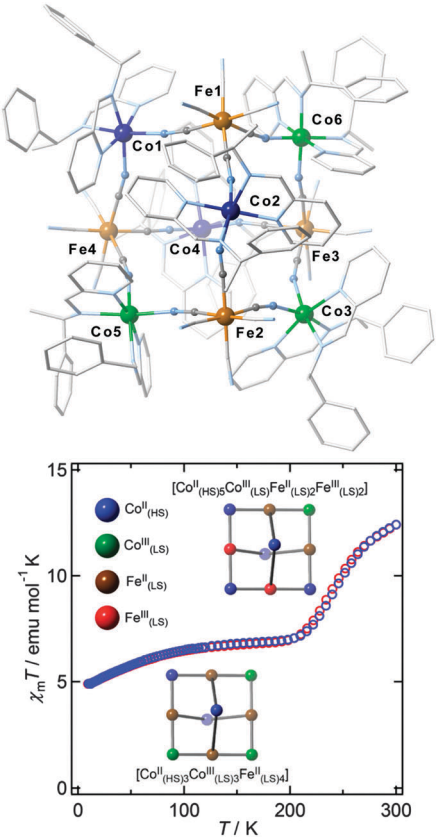

Fig. 9 (top) Representation of the molecular structure of $[NEt_4]_2\{[Co(L^R)]_6[Fe(CN)_6]_4\}[BF_4]\cdot 17CH_3OH\cdot 12H_2O$ (**29**) at T = 100 K. Hydrogen atoms, tetrafluoroborate and lattice-solvent molecules are omitted for clarity. Fe(II), Co(III), Co(II), N and C atoms are indicated in brown, green, dark blue, light blue and light grey, respectively. (bottom) χT *versus* T data cooling (blue dots) and heating (red dots) the sample, together with the diagrams of the spin state of each metal ion. Reprinted with permission from ref. 79. Copyright (2014) American Chemical Society.

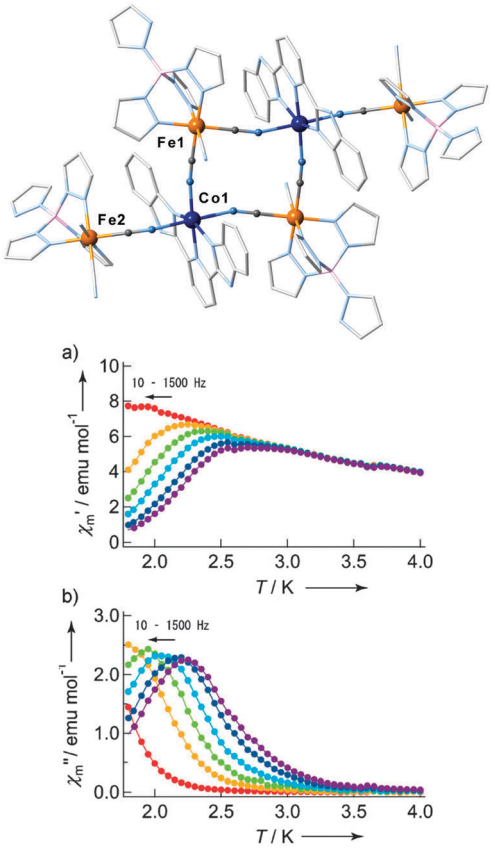

Fig. 10 (top) Representation of the molecular structure of $[Co_2Fe_4(bimpy)_2(CN)_6(\mu\text{-}CN)_6(pzTp)_4]\cdot 2(1\text{-}PrOH)\cdot 4H_2O$ (**30**) at T = 100 K. Hydrogen atoms and lattice-solvent molecules are omitted for clarity. Fe, Co, N, C, and B atoms are indicated in orange, dark blue, light blue, light grey, and pink, respectively. (bottom) χ' *versus* T (a) and χ'' *versus* T (b) data for compound **30** after light irradiation (H_{ac} = 3 Oe oscillating at 10–1500 Hz and H_{ext} = 500 Oe) demonstrating the slow relaxation of the magnetization in the light-induced paramagnetic phase. Reprinted with permission from ref. 81. Copyright 2012 Wiley-VCH.

iron centres: Fe^{II}_{LS} for the metal ions belonging to the central square (Fe1), and Fe^{III}_{LS} for the external ones (Fe2). In other words, these measurements suggested the occurrence of a thermally induced electron transfer between the iron and cobalt centres only within the central square core. This thermal conversion from $[Fe^{III}_{LS}(Co^{II}_{HS}Fe^{III}_{LS})_2Fe^{III}_{LS}]$ to $[Fe^{III}_{LS}(Co^{III}_{LS}Fe^{II}_{LS})_2Fe^{III}_{LS}]$ states was confirmed by magnetic susceptibility measurements, showing a characteristic decrease of the χT product centred around 220 K from high to low temperatures. When the sample was irradiated at 5 K (808 nm laser light), the χT value increased and reached saturation after about 150 minutes due to the intramolecular photo-induced electron transfer generating $[Fe^{III}_{LS}(Co^{II}_{HS}Fe^{III}_{LS})_2Fe^{III}_{LS}]$ species as confirmed by the 20 K crystal structures obtained before and after light irradiation. It is worth mentioning that the static magnetic properties of this photo-induced phase evidenced the presence of intramolecular ferromagnetic interactions between Co^{II}_{HS} and Fe^{III}_{LS} magnetic sites in contrast with the observation made in the three dimensional PBAs.[23,24,31] Below 4 K, the two accessible electronic configurations, the thermodynamics $[Fe^{III}_{LS}(Co^{III}_{LS}Fe^{II}_{LS})_2Fe^{III}_{LS}]$ and the photo-induced $[Fe^{III}_{LS}(Co^{II}_{HS}Fe^{III}_{LS})_2Fe^{III}_{LS}]$ ones, were studied by alternative current (ac) magnetic susceptibility measurements. While no evidence for slow dynamics of the magnetization was observed before irradiation, frequency dependence of the in-phase and out-of-phase signals under an external magnetic field of 500 Oe was clearly seen in the photo-induced phase (Fig. 10, bottom). From these measurements revealing the SMM properties of the light induced $[Fe^{III}_{LS}(Co^{II}_{HS}Fe^{III}_{LS})_2Fe^{III}_{LS}]$ phase in **30**, the relaxation time of the magnetization was estimated and found to follow a thermally activated law (*i.e.* Arrhenius law) with $\tau_0 = 5.7 \times 10^{-9}$ s and $\Delta_{eff}/k_B = 26$ K. Complex **30** is thus the first discrete molecule exhibiting slow relaxation of the magnetization in the light-induced phase.[81]

Another interesting example of multifunctional molecular cyanido-bridged Fe/Co complex exhibiting an electron transfer phenomenon was reported by Liu, Sato, Duan and coworkers.[82] In this case, the authors described a linear trinuclear compound, $\{[(Tp)Fe(CN)_3]_2Co(Meim)_4\}\cdot 6H_2O$ (**31**, Meim: *N*-methylimidazole), with the aim of controlling concomitantly the dielectric and the magnetic properties of the system. The reaction of $[NBu_4][(Tp)Fe(CN)_3]$ with $Co(NO_3)_2\cdot 6H_2O$ in the presence of Meim led to **31**, where a cobalt centre is inserted between two iron metal ions in a linear cyanido-bridged skeleton. At 240 K, the bond lengths around the metal ions observed in the crystal structure agreed well with a $[Fe^{III}_{LS}Co^{II}_{HS}Fe^{III}_{LS}]$ configuration. After cooling the sample at 150 K, a significant decrease of the bond distances around the Co site suggested a thermally induced electron transfer from the cobalt metal ion to one of the two iron centres (likely occurring randomly between the two iron sites) leading to a low temperature $[Fe^{II}_{LS}Co^{III}_{LS}Fe^{III}_{LS}]$ state. This conclusion was also supported by infrared and ^{57}Fe Mössbauer spectroscopies, from which the characteristics of the two iron configurations, Fe^{II}_{LS} and Fe^{III}_{LS}, were clearly observed. The thermal dependence of the magnetic susceptibility confirmed a reversible electron transfer transition (*i.e.* a first order phase transition) centred around 225 K with a small thermal hysteresis of about 10 K at 0.5 K min^{-1}. The χT values at high and low temperatures were found to be in good agreement with the expected electronic configurations. The possibility to photo-induce the electron transfer process was also demonstrated at 5 K by irradiating the sample with a laser source at 535 nm. This effect was found to be relatively inefficient in **31** with only about 20% of photo-conversion. The magnetic susceptibility measurements showed that this photo-induced $[Fe^{III}_{LS}Co^{II}_{HS}Fe^{III}_{LS}]$ fraction of the sample relaxed completely to the $[Fe^{III}_{LS}Co^{III}_{LS}Fe^{II}_{LS}]$ phase upon heating above 90 K.[82] In both thermally or photo-induced electron transfer processes for **31**, one electron from the single Co^{II}_{HS} site was transferred to one of the two Fe^{III}_{LS} centres. This phenomenon was thus imposing a change from a centrosymmetric nonpolar $[Fe^{III}_{LS}Co^{II}_{HS}Fe^{III}_{LS}]$ molecule into an asymmetric $[Fe^{III}_{LS}Co^{III}_{LS}Fe^{II}_{LS}]$ polar one, demonstrating the possibility to switch the polarity of a given complex by a "directional" electron transfer mechanism. Based on the X-ray crystal structures, DFT calculations were used to estimate the permanent electric dipole moment of the low temperature phase (18.4 D), and to demonstrate the

absence of dipole moment for the high temperature configuration. With this example, the authors demonstrated for the first time that it is possible to trigger a polar/nonpolar conversion of a molecular system by a thermally and photo-induced electron transfer mechanism.[82]

3.5. One and two-dimensional cyanido-bridged Fe/Co Prussian blue analogues with electron transfer properties

One and two-dimensional cyanido-bridged Fe/Co systems featuring metal-to-metal electron transfer properties have also been reported even if the number of examples in the literature is still very scarce.

The first example, $\{[(Tp)Fe(CN)_3]_2Co(bpe)\}\cdot 5H_2O$ (**32**·$5H_2O$), was described by Sato and co-workers in 2010.[83] This compound was synthesized by reacting $Li[(Tp)Fe(CN)_3]$ with $Co(NO_3)_2$ and 1,2-bis(4-pyridyl)ethane (bpe). This compound contains cyanido-bridged Fe/Co double zigzag chains (Fig. 11, top) with each cobalt centre linked to four $[(Tp)Fe(CN)_3]^-$ moieties which themselves act as a bidentate metallo-ligand between Co ions (Fig. 11, top). In the crystal structure, these chains are interconnected by the bpe ligands to form a two-dimensional framework. In addition, uncoordinated water molecules are located between the cyanido-bridged Fe/Co layers, interacting with them by significant hydrogen bonding interactions. At 223 K, the red crystals of **32**·$5H_2O$ exhibit a structure with metal–ligand bond distances indicating only paramagnetic Co^{II}_{HS} and Fe^{III}_{LS} sites. Lowering the temperature to 123 K, the structure of the thermochromic dark green crystals revealed the presence of randomly distributed Fe^{II}_{LS}, Fe^{III}_{LS}, Co^{II}_{HS} and Co^{III}_{LS} metal ions. This conclusion based on the metal–ligand bond distances was attributed to a partial intramolecular electron transfer as also supported by temperature-dependent IR spectroscopy, that showed reversibly the expected ν_{CN} bands at the different temperatures. The metal-to-metal electron transfer process was further confirmed by magnetic susceptibility studies. Above 220 K, the obtained χT value agreed well with only Fe^{III}_{LS} (two sites) and Co^{II}_{HS} (one site) magnetic centres (5.1 cm^3 K mol^{-1}; Fig. 11, bottom). Lowering the temperature, the χT product experienced a marked decrease around 180 K, before stabilizing down to about 1.9 cm^3 K mol^{-1} below 120 K. This low temperature value suggested that only two-thirds of the Co^{II}_{HS} metal ions are transformed into Co^{III}_{LS} sites. In addition to the thermally induced electron transfer phenomenon, the authors demonstrated that the high-temperature configuration can also be photo-generated at 5 K. After 12 hours of 532 nm light irradiation, the χT product raised notably. The resulting photo-induced phase was shown to relax to the original thermodynamic state upon heating the sample above 150 K. Interestingly, these thermally and photo-induced electron transfer phenomena exhibited by **32**·$5H_2O$ vanished after dehydrating the sample (Fig. 11, bottom). In both materials, **32**·$5H_2O$ and **32**, the magnetic properties revealed the occurrence of dominant ferromagnetic interactions between the paramagnetic metal ions (Fig. 11, bottom) as observed in **30**,[81] and again in contrast with the three dimensional PBAs.[23,24,31] Based on the crystal structure of **32** that

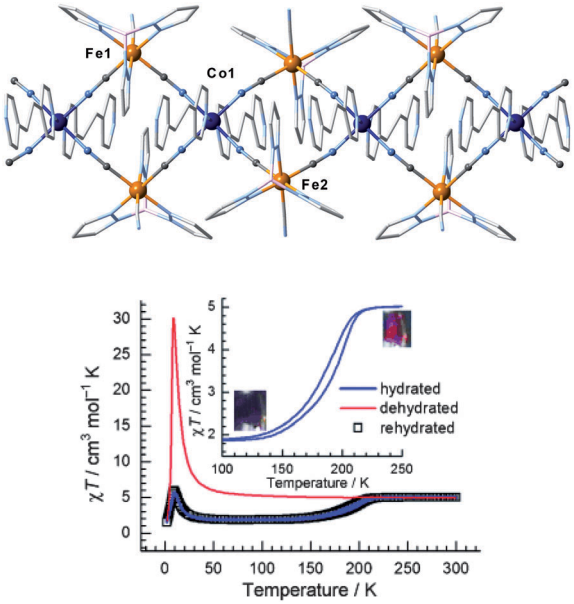

Fig. 11 (top) Representation of the molecular structure of $\{[(Tp)Fe(CN)_3]_2Co(bpe)\}\cdot 5H_2O$ (**32**·$5H_2O$) at T = 123 K. Hydrogen atoms and lattice-solvent molecules are omitted for clarity. Fe, Co, N, C, and B atoms are indicated in orange, dark blue, light blue, light grey, and pink, respectively. (bottom) χT *versus* T data of the hydrated (blue line), dehydrated (red line) and rehydrated (squares) of **32**. Reprinted with permission from ref. 83. Copyright 2010 Wiley-VCH.

established the complete removal of the water molecules observed in **32**·$5H_2O$, the authors attributed the absence of electron transfer properties in **32** to the lack of the water hydrogen bonding interactions toward terminal cyanido groups. This scenario suggests that the hydrogen bond network produced by the water molecules in **32**·$5H_2O$, pushes the redox potentials of the two metal ion sites to be close enough to favour the metal-to-metal electron transfer.[83] This "water-switchable" electron transfer system highlights once more the extreme sensitivity of the electron transfer process likely in link with redox potentials of the metal centres.

By changing the environment of the iron centre, the same group reported another two-dimensional compound **33**, $\{[Fe(bpy)(CN)_4]_2Co(4,4'\text{-bipyridine})\}\cdot 4H_2O$, exhibiting thermally and photo-induced electron transfer properties.[84] In this case, the authors used $Li[Fe(bpy)(CN)_4]$ as the iron precursor, while $Co(ClO_4)_2$ and 4,4′-bipyridine were chosen to assemble the cobalt counterpart. As in **32**·$5H_2O$ (Fig. 11, top), the crystal structure shows a double zigzag chain conformation, with the cobalt metal ions connected by four cyanide groups to four $[Fe(bpy)(CN)_4]$ moieties. Two 4,4′-bipyridine ligands complete the Co coordination sphere and connect the chains into a 2D network. As already observed in **32**·$5H_2O$, water molecules are intercalated between the cyanido/bpy-bridged Fe/Co layers. Partial thermally (around 215 K) and light-induced electron transfer phenomena were characterized by X-ray diffraction, infrared spectroscopy, magnetic measurements and recently by X-ray absorption spectroscopy.[84b] Interestingly, strong frequency dependence of the ac susceptibility (for both in-phase and

out-of-phase components) was observed in the photo-induced metastable state of **33**. The relaxation time of the dynamics was shown to follow an Arrhenius law with an energy barrier of 29 K and a pre-exponential factor of 1.4×10^{-9} s. Based on a qualitative analysis of the magnetic data, the authors attributed the observed slow dynamics of the magnetization to the intrinsic Single-Chain Magnet (SCM)[85] properties of the chains in the antiferromagnetically ordered phase (T_N = 3.8 K).

In order to minimize the inter-chain magnetic interactions and obtain a SCM system, the authors recently proposed to use other ligands able to separate more efficiently the $\{Fe_2Co\}_\infty$ chains. This strategy is well illustrated by complex **34**, $\{[(pzTp)Fe(CN)_3]_2Co(4\text{-styrylpyridine})_2\}\cdot 2H_2O\cdot 2CH_3OH$.[86] In this case, Liu, Sato, Duan and co-workers used a bulkier pzTp ligand to block the iron centre, while a monodentate ligand (4-styrylpyridine) was chosen to complete the coordination of the cobalt ion. Consequently, **34** exhibits an one-dimensional structural organization with double zigzag chains (similar to **32**·5H_2O in Fig. 11, top), which are not connected (in contrast to **32**·5H_2O and **33**) but just separated by uncoordinated water molecules. In this case, crystallographic, spectroscopic and magnetic techniques confirmed a full thermally induced electron transfer around 230 K from Fe^{III}_{LS}–CN–Co^{II}_{HS} pairs to Fe^{II}_{LS}–CN–Co^{III}_{LS} ones while decreasing the temperature. As the stoichiometry of compound **34** is one cobalt for two Fe centres, only half of the iron metal ions are involved in the electron transfer process with all Co sites. Surprisingly, this phenomenon engaged specifically one of the two iron sites instead of randomly involving both iron centres as described for example in the trinuclear complex **31**.[82] The authors attributed this ordered electron transfer to the presence of different hydrogen bonding interactions around the two $[(pzTp)Fe(CN)_3]^{2-}$ units with the solvent molecules in the crystal packing. The photo-induced electron transfer was first shown in **34** by infrared spectroscopy and the decrease of the bridging ν_{CN} absorption peaks from the $Fe^{II/III}_{LS}$–CN–Co^{III}_{LS} units after a 532 nm laser irradiation of the sample. Magnetic measurements further confirmed the photoactivity of the sample. After an irradiation of 12 hours at 5 K, the χT product was significantly increased as expected for the photoconversion of a material composed essentially of isolated paramagnetic Fe^{III}_{LS} centres to an one-dimensional magnetically correlated $\{(Fe^{III}_{LS})_2Co^{II}_{HS}\}_\infty$ system. The magnetization dynamics of these metastable photo-induced chains was studied by ac magnetic susceptibility measurements, which revealed a thermally activated relaxation time with an energy barrier of 27 K ($\tau_0 = 1.4 \times 10^{-10}$ s). Based solely on the study of the magnetization dynamics, the authors concluded to the photo-induced SCM properties of **34**. In addition, the thermal relaxation of the metastable photo-induced state was studied by monitoring the time decay of the magnetization at different temperatures. Above 40 K, the photo-generated phase relaxed with an Arrhenius behaviour and an energy barrier of 1348 ± 200 cm^{-1} (1926 ± 286 K) ($\tau_0 = 8.4 \times 10^{-12}$ s). In contrast at lower temperatures (<40 K), a temperature independent tunnelling relaxation of the excited paramagnetic $\{(Fe^{III}_{LS})_2Co^{II}_{HS}\}_\infty$ state to the $\{Fe^{III}_{LS}Fe^{II}_{LS}Co^{III}_{LS}\}_\infty$ ground state was observed. Overall, this remarkable compound constitutes the first evidence of the possibility to design photo-switchable single-chain magnets from one-dimensional cyanido-bridged Fe/Co Prussian blue analogues based on a metal-to-metal electron transfer mechanism.[86]

In 2012, Oshio and co-workers reported another type of one dimensional cyanido-bridged Fe/Co compound with a chiral square-wave chain topology: $\{[Co^{II}((R)\text{-pabn})][(Tp)Fe^{III}(CN)_3]\}\cdot(BF_4)\cdot MeOH\cdot 2H_2O$ (**35*R***·MeOH·2H_2O; (*R*)-pabn: (*R*)-*N*(2),*N*(2′)-bis(pyridine-2-ylmethyl)-1,1′-binaphtyl-2,2′-diamine), and $\{[Co^{II}((S)\text{-pabn})][(Tp)Fe^{III}(CN)_3]\}(BF_4)\cdot 2H_2O$ (**35*S***·2H_2O).[87] By reacting $[NBu_4][(Tp)Fe(CN)_3]$ with the corresponding cobalt building block ($[Co^{II}((R)\text{-pabn})]^{2+}$ or $[Co^{II}((S)\text{-pabn})]^{2+}$), the authors were able to synthesize both enantiomerically pure materials. These cyanido-bridged Fe/Co chain systems crystalized in the chiral $P2_12_12_1$ space group, with the cobalt metal ions chelated by four N atoms from the pabn ligand and linked to two cyanide N atoms from the iron $[(Tp)Fe(CN)_3]^-$ units (Fig. 12, top). Compound **35*R***·MeOH·2H_2O was found to lose the solvated methanol molecules and evolves to **35*R***·H_2O (when dried under N_2) or to **35*R***·3H_2O (when dried in air). While the magnetic properties of both *R* and *S* enantiomers were found, as expected, to be the same, the different solvated systems showed a thermally induced electron transfer phenomenon with a thermal hysteretic behaviour differing only by the $T_{1/2}$ values (above 250 K). These materials appeared to be fully diamagnetic at low temperatures in agreement with the $\{Fe^{II}_{LS}Co^{III}_{LS}\}_\infty$ ground state and exhibited χT values (*ca.* 3.4 cm^3 $K\ mol^{-1}$) coherent with the paramagnetic $\{Fe^{III}_{LS}Co^{II}_{HS}\}_\infty$ phase above the thermal hysteresis.[87] These metal-to-metal electron transfer properties were also confirmed by Mössbauer spectroscopy and single-crystal X-ray diffraction experiments. In addition, the temperature dependence of the electrical properties of **35*R***·H_2O was probed. Below 250 K, the value of the electrical conductivity was found to be around 10^{-12} S m^{-1}, suggesting an insulating state. By increasing the temperature above the electron transfer temperature, the conductivity raised to about 10^{-9} S m^{-1} with semiconducting properties in the paramagnetic phase. Similarly to the magnetic properties, conductivity measurements exhibited a thermal hysteresis associated to the electron transfer process, thus demonstrating that **35*R***·H_2O possessed not only magnetic but also electric bistability (Fig. 12, bottom). As well, the photomagnetic properties of **35*R***·H_2O were studied by irradiating the sample with an 808 nm laser at 5 K. Under light, a fast increase of the χT values (up to *ca.* 300 cm^3 $K\ mol^{-1}$) was detected suggesting the photo-generation of the metastable paramagnetic $\{Fe^{III}_{LS}Co^{II}_{HS}\}_\infty$ state. The χT *vs.* *T* data revealed the presence of ferromagnetic interactions between Fe^{III}_{LS} and Co^{II}_{HS} magnetic sites within the photo-induced state, which relaxed to the diamagnetic ground state when the temperature exceeded 72 K. Furthermore, the characterization of the photo-generated $\{Fe^{III}_{LS}Co^{II}_{HS}\}_\infty$ state was carried out by ac susceptibility measurements showing a strong frequency-dependence of both in-phase and out-of-phase signals. Two thermally activated relaxation processes of the magnetization were identified with energy barriers of 65.5 K ($\tau_0 = 3.1 \times 10^{-10}$ s^{-1}) and 33.3 K ($\tau_0 = 1.1 \times 10^{-8}$ s^{-1}). Without further analysis of the

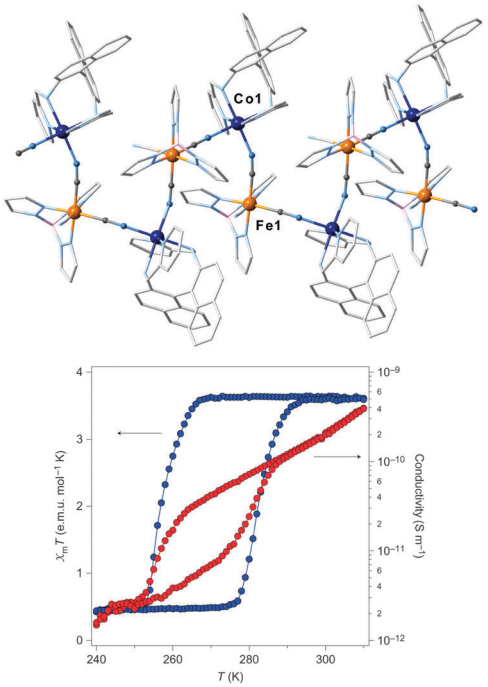

Fig. 12 (top) Representation of the one-dimensional structure of $[Co^{II}((R)\text{-pabn})][(Tp)Fe^{III}(CN)_3](BF_4)\cdot MeOH\cdot 2H_2O$ (**35*R***·MeOH·2H_2O) shown at 360 K. Hydrogen atoms, tetrafluoroborate and lattice-solvent molecules are omitted for clarity. Fe, Co, N, C, and B atoms are indicated in orange, dark blue, light blue, light grey, and pink, respectively. (bottom) Temperature dependence of the χT product (blue dots) and the dc conductivity (red dots) of **35*R***·H_2O. Reprinted with permission from ref. 87. Copyright (2012) Nature Chemistry, McMillan Publishers Ltd.

static magnetic susceptibility, the authors concluded from this dynamic study that the photo-induced state displayed single-chain magnet properties. Thanks to thermally and light-induced electron transfer processes, this multifunctional material displays above 250 K both magnetic and conductivity bistabilities in temperature, while below 10 K, a photo-induced "tristability" (from the diamagnetic state and the field-induced ±M states from the SCM properties) is also described.[87]

Recently, Nojiri, Oshio and co-workers showed that the solid state grinding of **35*R***·MeOH·2H_2O could also provoked an electron transfer and thus switched its diamagnetic state to the paramagnetic phase.[88] This new way of inducing the metal-to-metal electron transfer was indeed associated to the partial dehydration of the sample (*i.e.* the loss of only one water molecule) as deduced by thermogravimetric experiments. L-edge XAS and XMCD measurements were performed to characterize the different phases before and after grinding the sample and confirmed the observed effect. This study highlighted once more the key role of the interstitial solvent molecules on the metal-to-metal electron transfer process.

4. Conclusions and outlook

The different examples presented in this review article illustrate the diversity of Fe/Co Prussian blue analogues from extended networks to molecular systems, which have been synthesized from serendipitous or by-design coordination chemistry. The remarkable research work on the tridimensional cyanido-bridged Fe/Co PBA networks has been essential to improve the comprehension of the metal-to-metal electron transfer process but also to access to a certain degree of control of their physical properties. In that sense, the subtle compromise between the number of diamagnetic Fe^{II}_{LS}–CN–Co^{III}_{LS} units present in these 3D systems and the network flexibility, modulated by the iron vacancies, can be considered as the first important conclusion of these studies in order to explain and fine tune the thermally and photo-induced electron transfer phenomena. However, the disordered nature and heterogeneity of these materials together with their low solubility reflect the difficulties that must be overcome to envisage some possible applications. These aspects are absent, or almost absent, in the molecular or low dimensional cyanido-bridged Fe/Co systems. Then the detailed study of the electron transfer phenomena appears always easier in these molecule-based compounds by simply analysing their structures from a single crystal at different temperatures or before/after irradiation, but also by probing in solution the redox properties (of the building blocks and/or the final product), which turned to be the most important information to understand and control the observed physical behaviours. As the redox potentials at each metal ion site are highly influenced by their respective coordination spheres and thus by the organic capping ligands, chemists have use this knowledge to develop new synthetic strategies with custom-made ligands. As a result, these designed molecular or low dimensional systems display adjustable physical properties with improved characteristics in comparison to their tridimensional analogues. In the last few years, the scientific community has made an important effort of research on these Fe/Co PBAs reporting more and more examples, which demonstrate the interest and potential behind these new molecular or low dimensional complexes. Consequently, the understanding of the metal-to-metal electron transfer process in these systems has progressed tremendously. Nowadays, researchers can design complexes with magnetic and optical bistabilities induced by an electron transfer, but also can combine those with other physical properties allowing their thermal or light control and leading to a new generation of multifunctional materials. Over time with the synthesis of easily processable molecular PBAs and the development of new technologies based on molecules, these multifunctional complexes and their astonishing switchable physical properties will certainly find their use in future high-tech devices.

Acknowledgements

This work was supported by the University of Bordeaux, the CNRS, the Aquitaine Region, the Institut Universitaire de France and the ANR (ANR-12-PDOC-0038).

Notes and references

1 D. Gatteschi and R. Sessoli, *Angew. Chem., Int. Ed.*, 2003, **42**, 268.
2 C. Coulon, H. Miyasaka and R. Clérac, *Struct. Bonding*, 2006, **122**, 163.
3 M. Verdaguer and G. Girolami, in *Magnetism – Molecules to Materials*, ed. J. S. Miller and M. Drillon, Wiley-VCH, Weinheim, 2004, vol. 5, p. 283.
4 P. Gütlich, A. Hauser and H. Spiering, *Angew. Chem., Int. Ed. Engl.*, 1994, **33**, 2024.
5 O. Sato, J. Tao and Y.-Z. Zhang, *Angew. Chem., Int. Ed.*, 2007, **46**, 2152.
6 O. Sato, *J. Photochem. Photobiol., C*, 2004, **5**, 203.
7 S. Decurtins, P. Gütlich, C. P. Köhler, H. Spiering and A. Hauser, *Chem. Phys. Lett.*, 1984, **105**, 1.
8 M. Natali, S. Campagna and F. Scandola, *Chem. Soc. Rev.*, 2014, **43**, 4005.
9 A. Bleuzen, V. Marvaud, C. Mathonière, B. Sieklucka and M. Verdaguer, *Inorg. Chem.*, 2009, **48**, 3453.
10 S.-i. Ohkoshi and H. Tokoro, *Acc. Chem. Res.*, 2012, **45**, 1749.
11 N. Shimamoto, S.-i. Ohkoshi, O. Sato and K. Hashimoto, *Inorg. Chem.*, 2002, **41**, 678.
12 T. Mallah, C. Auberger, M. Verdaguer and P. Veillet, *J. Chem. Soc., Chem. Commun.*, 1995, 61.
13 J.-N. Rebilly and T. Mallah, *Struct. Bonding*, 2006, **122**, 103.
14 L. M. C. Beltran and J. R. Long, *Acc. Chem. Res.*, 2005, **38**, 325.
15 R. Lescouëzec, L. M. Toma, J. Vaissermann, M. Verdaguer, F. S. Delgado, C. Ruiz-Pérez, F. Lloret and M. Julve, *Coord. Chem. Rev.*, 2005, **249**, 2691.
16 K. S. Pedersen, J. Bendix and R. Clérac, *Chem. Commun.*, 2014, **50**, 4396.
17 M. B. Robin, *Inorg. Chem.*, 1962, **1**, 337.
18 M. B. Robin and P. Day, in *Adv. Inorg. Chem. Radiochem.*, ed. H. J. Emeléus and A. G. Sharpe, Academic Press, 1968, vol. 10, p. 247.
19 A. Ludi and H. U. Güdel, *Struct. Bonding*, 1973, **14**, 1.
20 H. J. Buser, D. Schwarzenbach, W. Petter and A. Ludi, *Inorg. Chem.*, 1977, **16**, 2704.
21 F. Herren, P. Fischer, A. Ludi and W. Haelg, *Inorg. Chem.*, 1980, **19**, 956.
22 O. Sato, T. Iyoda, A. Fujishima and K. Hashimoto, *Science*, 1996, **272**, 704.
23 A. Bleuzen, C. Lomenech, V. Escax, F. Villain, F. Varret, C. Cartier dit Moulin and M. Verdaguer, *J. Am. Chem. Soc.*, 2000, **122**, 6648.
24 V. Escax, A. Bleuzen, C. Cartier dit Moulin, F. Villain, A. Goujon, F. Varret and M. Verdaguer, *J. Am. Chem. Soc.*, 2001, **123**, 12536.
25 J.-D. Cafun, G. Champion, M.-A. Arrio, C. C. dit Moulin and A. Bleuzen, *J. Am. Chem. Soc.*, 2010, **132**, 11552.
26 M. Verdaguer, *Science*, 1996, **272**, 698.
27 O. Sato, Y. Einaga, T. Iyoda, A. Fujishima and K. Hashimoto, *J. Electrochem. Soc.*, 1997, **144**, L11.
28 Y. Einaga, O. Sato, T. Iyoda, Y. Kobayashi, F. Ambe, K. Hashimoto and A. Fujishima, *Chem. Lett.*, 1997, 289.
29 O. Sato, Y. Einaga, T. Iyoda, A. Fujishima and K. Hashimoto, *J. Phys. Chem. B*, 1997, **101**, 3903.
30 Y. Einaga, S.-i. Ohkoshi, O. Sato, A. Fujishima and K. Hashimoto, *Chem. Lett.*, 1998, 585.
31 O. Sato, Y. Einaga, A. Fujishima and K. Hashimoto, *Inorg. Chem.*, 1999, **38**, 4405.
32 D. A. Pejaković, J. L. Manson, J. S. Miller and A. J. Epstein, *J. Appl. Phys.*, 2000, **87**, 6028.
33 D. A. Pejaković, J. L. Manson, J. S. Miller and A. J. Epstein, *Phys. Rev. Lett.*, 2000, **85**, 1994.
34 A. Goujon, F. Varret, V. Escax, A. Bleuzen and M. Verdaguer, *Polyhedron*, 2001, **20**, 1339.
35 A. Bleuzen, C. Lomenech, A. Dolbecq, F. Villain, A. Goujon, O. Roubeau, M. Nogues, F. Varret, F. Baudelet, E. Dartyge, C. Giorgetti, J.-J. Gallet, C. C. D. Moulin and M. Verdaguer, *Mol. Cryst. Liq. Cryst.*, 1999, **335**, 253.
36 A. Goujon, O. Roubeau, F. Varret, A. Dolbecq, A. Bleuzen and M. Verdaguer, *Eur. Phys. J. B*, 2000, **14**, 115.
37 A. Goujon, F. Varret, V. Escax, A. Bleuzen and M. Verdaguer, *Polyhedron*, 2001, **20**, 1347.
38 C. Cartier dit Moulin, G. Champion, J.-D. Cafun, M.-A. Arrio and A. Bleuzen, *Angew. Chem., Int. Ed.*, 2007, **46**, 1287.
39 V. Escax, A. Bleuzen, J. P. Itié, P. Munsch, F. Varret and M. Verdaguer, *J. Phys. Chem. B*, 2003, **107**, 4763.
40 N. Shimamoto, S. Ohkoshi, O. Sato and K. Hashimoto, *Mol. Cryst. Liq. Cryst.*, 2000, **344**, 95.
41 S. Gawali-Salunke, F. Varret, I. Maurin, C. Enachescu, M. Malarova, K. Boukheddaden, E. Codjovi, H. Tokoro, S.-i. Ohkoshi and K. Hashimoto, *J. Phys. Chem. B*, 2005, **109**, 8251.
42 R. Le Bris, J.-D. Cafun, C. Mathonière, A. Bleuzen and J.-F. Letard, *New J. Chem.*, 2009, **33**, 1255.
43 T. Yokoyama, T. Ohta, O. Sato and K. Hashimoto, *Phys. Rev. B: Condens. Matter Mater. Phys.*, 1998, **58**, 8257.
44 A. Bleuzen, V. Escax, A. Ferrier, F. Villain, M. Verdaguer, P. Münsch and J.-P. Itié, *Angew. Chem., Int. Ed.*, 2004, **43**, 3728.
45 C. Cartier dit Moulin, F. Villain, A. Bleuzen, M.-A. Arrio, P. Sainctavit, C. Lomenech, V. Escax, F. Baudelet, E. Dartyge, J.-J. Gallet and M. Verdaguer, *J. Am. Chem. Soc.*, 2000, **122**, 6653.
46 G. Champion, V. Escax, C. Cartier dit Moulin, A. Bleuzen, F. Villain, F. Baudelet, E. Dartyge and M. Verdaguer, *J. Am. Chem. Soc.*, 2001, **123**, 12544.
47 T. Yokoyama, M. Kiguchi, T. Ohta, O. Sato, Y. Einaga and K. Hashimoto, *Phys. Rev. B: Condens. Matter Mater. Phys.*, 1999, **60**, 9340.
48 E. Dujardin, S. Ferlay, X. Phan, C. Desplanches, C. Cartier dit Moulin, P. Sainctavit, F. Baudelet, E. Dartyge, P. Veillet and M. Verdaguer, *J. Am. Chem. Soc.*, 1998, **120**, 11347.
49 P. V. Bernhardt and M. Martinez, *Inorg. Chem.*, 1999, **38**, 424.
50 R. E. Hester and E. M. Nour, *J. Chem. Soc., Dalton Trans.*, 1981, 939.
51 P. V. Bernhardt, B. P. Macpherson and M. Martinez, *J. Chem. Soc., Dalton Trans.*, 2002, 1435.

52 A. Vogler and H. Kunkely, *Ber. Bunsen-Ges. Phys. Chem.*, 1975, **79**, 301.
53 S.-Z. Zhan, X.-Y. Chen, Q.-J. Meng and W. Xie, *Synth. React. Inorg. Met.-Org. Chem.*, 1996, **26**, 277.
54 C. P. Berlinguette, A. Dragulescu-Andrasi, A. Sieber, J. R. Galán-Mascarós, H.-U. Güdel, C. Achim and K. R. Dunbar, *J. Am. Chem. Soc.*, 2004, **126**, 6222.
55 C. P. Berlinguette, A. Dragulescu-Andrasi, A. Sieber, H.-U. Güdel, C. Achim and K. R. Dunbar, *J. Am. Chem. Soc.*, 2005, **127**, 6766.
56 K. E. Funck, A. V. Prosvirin, C. Mathonière, R. Clérac and K. R. Dunbar, *Inorg. Chem.*, 2011, **50**, 2782.
57 D. Li, R. Clérac, O. Roubeau, E. Harté, C. Mathonière, R. Le Bris and S. M. Holmes, *J. Am. Chem. Soc.*, 2008, **130**, 252.
58 J. L. Heinrich, P. A. Berseth and J. R. Long, *Chem. Commun.*, 1998, 1231.
59 K. K. Klausmeyer, T. B. Rauchfuss and S. R. Wilson, *Angew. Chem., Int. Ed.*, 1998, **37**, 1694.
60 H. Oshio, H. Onodera, O. Tamada, H. Mizutani, T. Kikichi and T. Ito, *Chem. – Eur. J.*, 2000, **6**, 2523.
61 Y. Zhang, D. Li, R. Clérac, M. Kalisz, C. Mathonière and S. M. Holmes, *Angew. Chem., Int. Ed.*, 2010, **49**, 3752.
62 G. N. Newton, M. Nihei and H. Oshio, *Eur. J. Inorg. Chem.*, 2011, 3031.
63 M. Nihei, Y. Sekine, N. Suganami and H. Oshio, *Chem. Lett.*, 2010, 978.
64 (*a*) M. Nihei, Y. Sekine, N. Suganami, K. Nakazawa, A. Nakao, H. Nakao, Y. Murakami and H. Oshio, *J. Am. Chem. Soc.*, 2011, **133**, 3592; (*b*) Y. Kitagawa, M. Asaoka, K. Miyagi, T. Matsui, M. Nihei, H. Oshio, M. Okumura and M. Nakano, *Inorg. Chem. Front.*, 2015, **2**, 771.
65 Y. Sekine, M. Nihei, R. Kumai, H. Nakao, Y. Murakami and H. Oshio, *Inorg. Chem. Front.*, 2014, **1**, 540.
66 Y. Sekine, M. Nihei, R. Kumai, H. Nakao, Y. Murakami and H. Oshio, *Chem. Commun.*, 2014, **50**, 4050.
67 D. Siretanu, D. Li, L. Buisson, D. M. Bassani, S. M. Holmes, C. Mathonière and R. Clérac, *Chem. – Eur. J.*, 2011, **17**, 11704.
68 D. Li, S. Parkin, G. Wang, G. T. Yee, A. V. Prosvirin and S. M. Holmes, *Inorg. Chem.*, 2005, **44**, 4903.
69 Y. Sekine, M. Nihei and H. Oshio, *Chem. Lett.*, 2014, **43**, 1029.
70 Y.-Z. Zhang, P. Ferko, D. Siretanu, R. Ababei, N. P. Rath, M. J. Shaw, R. Clérac, C. Mathonière and S. M. Holmes, *J. Am. Chem. Soc.*, 2014, **136**, 16854.
71 (*a*) L. Cao, J. Tao, Q. Gao, T. Liu, Z. Xia and D. Li, *Chem. Commun.*, 2014, **50**, 1665; (*b*) C. Zheng, J. Xu, Z. Yang, J. Tao and D. Li, *Inorg. Chem.*, 2015, **54**, 9687.
72 J. Mercurol, Y. Li, E. Pardo, O. Risset, M. Seuleiman, H. Rousselière, R. Lescouëzec and M. Julve, *Chem. Commun.*, 2010, **46**, 8995.
73 A. Mondal, Y. Li, M. Seuleiman, M. Julve, L. Toupet, M. Buron-Le Cointe and R. Lescouëzec, *J. Am. Chem. Soc.*, 2013, **135**, 1653.
74 P. V. Bernhardt, B. P. Macpherson and M. Martinez, *Inorg. Chem.*, 2000, **39**, 5203.
75 B. P. Macpherson, P. V. Bernhardt, A. Hauser, S. Pagès and E. Vauthey, *Inorg. Chem.*, 2005, **44**, 5530.
76 I.-R. Jeon, S. Calancea, A. Panja, D. M. Pinero Cruz, E. S. Koumousi, P. Dechambenoit, C. Coulon, A. Wattiaux, P. Rosa, C. Mathonière and R. Clérac, *Chem. Sci.*, 2013, **4**, 2463.
77 E. S. Koumousi, I.-R. Jeon, Q. Gao, P. Dechambenoit, D. N. Woodruff, P. Merzeau, L. Buisson, X. Jia, D. Li, F. Volatron, C. Mathonière and R. Clérac, *J. Am. Chem. Soc.*, 2014, **136**, 15461.
78 K. Mitsumoto, E. Oshiro, H. Nishikawa, T. Shiga, Y. Yamamura, K. Saito and H. Oshio, *Chem. – Eur. J.*, 2011, **17**, 9612.
79 T. Shiga, T. Tetsuka, K. Sakai, Y. Sekine, M. Nihei, G. N. Newton and H. Oshio, *Inorg. Chem.*, 2014, **53**, 5899.
80 D. Gatteschi and R. Sessoli, *Angew. Chem., Int. Ed.*, 2003, **42**, 268.
81 M. Nihei, Y. Okamoto, Y. Sekine, N. Hoshino, T. Shiga, I. P.-C. Liu and H. Oshio, *Angew. Chem., Int. Ed.*, 2012, **51**, 6361.
82 T. Liu, D.-P. Dong, S. Kanegawa, S. Kang, O. Sato, Y. Shiota, K. Yoshizawa, S. Hayami, S. Wu, C. He and C.-Y. Duan, *Angew. Chem., Int. Ed.*, 2012, **51**, 4367.
83 T. Liu, Y.-J. Zhang, S. Kanegawa and O. Sato, *Angew. Chem., Int. Ed.*, 2010, **49**, 8645.
84 (*a*) T. Liu, Y.-J. Zhang, S. Kanegawa and O. Sato, *J. Am. Chem. Soc.*, 2010, **132**, 8250; (*b*) J. Yang, L. Zhou, J. Cheng, Z. Hu, C. Kuo, C.-W. Pao, L. Jang, J.-F. Lee, J. Dai, S. Zhang, S. Feng, P. Kong, Z. Yuan, J. Yuan, Y. Uwatoko, T. Liu, C. Jin and Y. Long, *Inorg. Chem.*, 2015, **54**, 6433.
85 C. Coulon, H. Miyasaka and R. Clérac, *Struct. Bonding*, 2006, **122**, 1; C. Coulon, V. Pianet, M. Urdampilleta and R. Clérac, *Struct. Bonding*, 2015, **164**, 143.
86 D.-P. Dong, T. Liu, S. Kanegawa, S. Kang, O. Sato, C. He and C.-Y. Duan, *Angew. Chem., Int. Ed.*, 2012, **51**, 5119.
87 N. Hoshino, F. Iijima, G. N. Newton, N. Yoshida, T. Shiga, H. Nojiri, A. Nakao, R. Kumai, Y. Murakami and H. Oshio, *Nat. Chem.*, 2012, **4**, 921.
88 M. L. Baker, Y. Kitagawa, T. Nakamura, K. Tazoe, Y. Narumi, Y. Kotani, F. Iijima, G. N. Newton, M. Okumura, H. Oshio and H. Nojiri, *Inorg. Chem.*, 2013, **52**, 13956.

